Dynamical Climatology

Non-linear effects on heat-induced circulation of the tropical atmosphere.

by

A.E. Gill and P.J. Phlips

DCTN 21 March 1985

Meteorological Office (Met. O. 20)
London Road
Bracknell
Berkshire RG12 2SZ

DYNAMICAL CLIMATOLOGY TECHNICAL NOTE NO. 21

NON-LINEAR EFFECTS ON HEAT-INDUCED CIRCULATION OF THE TROPICAL ATMOSPHERE

by

A E Gill

Meteorological Office, Hooke Institute, Oxford

and

P J Phlips

Oxford University, Hooke Institute, Oxford

Submitted for publication in Quart. J. Roy. Meteorol. Soc.

Met O 20 (Dynamical
Climatology Branch)
Meteorological Office
London Road
Bracknell
Berkshire, U.K. RG12 2SZ

March 1985

Note: This paper has not been published. Permission to quote from it should be obtained from the Assistant Director of the above Meteorological Office Branch.

NON-LINEAR EFFECTS ON HEAT-INDUCED CIRCULATION OF THE TROPICAL ATMOSPHERE

by A.E. Gill* and P.J. Phlips**

Hooke Institute, Clarendon Laboratory, Oxford OX1 3PU

A non-linear model of the atmospheric response to an isolated region of heating centred on the equator is constructed by expanding in a small amplitude parameter. In order to emphasize non-linear effects relative to frictional ones, the asymptotics of the small friction limit are first derived, and this limiting solution is used on the first term in the expansion with respect to the amplitude parameter. Compared with the linear solution, the non-linear solution has more inflow from the west at the surface and a reduced easterly outlfow at the tropopause. Moreover the pressure is reduced when velocities are large because of the Bernoulli effect. The conclusions are in good general agreement with the numerical results of Nobre (1983) and the observational study of Sardeshmukh and Hoskins (1985).

* Meteorological Office

** Oxford University

1. Introduction

Linear models of the large-scale heat-induced circulation of the tropical atmosphere have proved to work remarkably well and be a useful aid to understanding the primary observed features of the circulation.

The models are driven by a specified heat source representing diabatic heating due to latent heat release, and examples can be found in the work of Matsuno (1966), Webster (1972) and Gill (1980). Applications of the simple modelling approach have been described, e.g. Moura and Shukla (1981) have shown its usefulness for understanding the effect of sea-surface temperature anomalies in the Atlantic on droughts in NE Brazil, Lau and Lim (1982) have used the technique to study the winter monsoon, and Gill and Rasmusson (1983) have used the model to study the 1982/3 warm event in the equatorial Pacific. Transient phenomena have been studied by Heckley and Gill (1984) and by Silva Dias et al. (1984).

However large wind anomalies of 10 ms^{-1} at the surface and 20 ms^{-1} at the tropopause are observed e.g. in El Nino conditions, and these anomalies are not small compared with the propogation speed of the fastest waves of order 50 ms^{-1}. Furthermore observational studies such as that of Sardeshmukh and Hoskins (1985) clearly show the importance of non-linearity. These facts provide the motivation for the present study.

The basic idea was to use the linear model of Gill (1980) as a starting point and to examine how the solution is distorted as the amplitude of the forcing is increased. The linear solution already contains one small parameter ϵ which measures the importance of friction, so when another small parameter δ is introduced as a measure of

Cont/d

the amplitude, the question is raised as to the relative importance of these two parameters. In this study, the approach adopted is to make the amplitude parameter much larger than the frictional one so that non-linear effects will be more important than friction. This leads to the idea of first examining the limit of vanishingly small friction and this is done in sections 3 and 4. In this limit, there is an inner heating region of fixed dimensions and outer decay regions to both east and west whose longitudinal dimensions become infinitely large as friction becomes vanishingly small. The small friction limit is then used as the first term in an expansion in powers of the amplitude parameter δ.

The linear solution has a sinusoidal structure in the vertical so the non-linear terms involve a harmonic part and a height-independent part. The latter generates a barotropic non-linear correction to the linear solution (section 7) and the former a second baroclinic component (section 8). It turns out that the non-linear modifications are largest near the western end of the heating zone, and these modifications are discussed in section 9. The pressure is reduced substantially by the Bernoulli effect and other aspects of the non-linearity can be understood in terms of the absolute vorticity balance. As an introduction to this discussion, the total vorticity field corresponding to the linear solution is examined in an earlier section (section 5).

Finally, comparisons with the numerical results of Nobre (1983) and the analysis of observations by Sardeshmukh and Hoskins (1985) is made in section 10. The picture that emerges is that non-linear effects are quite important in practice, but their effect is to produce modest distortions of the flow rather than any fundamental change in character.

Cont/d

The nature of these distortions is well represented by the analytic results of this paper. The non-linear flow fields do not look greatly different from the linear ones and the magnitudes of the velocities are similar, and this is a major reason why the linear theories have been so successful.

2. Equations and Scalings

The equations of the model are

$$\underline{u}.\nabla u - \beta y v = -\partial\phi/\partial x - r u \tag{2.1}$$

$$\underline{u}.\nabla v + \beta y u = -\partial\phi/\partial y - r v \tag{2.2}$$

$$\underline{u}.\nabla\theta + w\, d\Theta/dz = Q - r\theta \tag{2.3}$$

$$\partial\phi/\partial z = g\theta/\Theta_0 \tag{2.4}$$

$$\partial u/\partial x + \partial v/\partial y + \partial w/\partial z = 0 \tag{2.5}$$

$$N^2 = \frac{g}{\Theta_0}\frac{d\Theta}{dz} \tag{2.6}$$

The equations can be put in nondimensional form by defining non-dimensional variables as follows

$$x_* = x/l \qquad y_* = y/a \qquad z_* = z/H$$

$$u_* = u/u_0 \qquad v_* = v/v_0 \qquad w_* = w/w_0$$

$$\phi_* = \phi/\phi_0 \qquad \theta_* = \theta/\theta_0 \qquad Q_* = Q/Q_0$$

where Q_0 is a given measure of the heating rate, H is a given vertical scale, l is a given measure of the zonal extent of the heating region, and a is the equatorial Rossby radius given by

$$a = (NH/2\beta)^{1/2} \tag{2.7}$$

In this paper, H will be chosen so that $NH = c$, the speed of long gravity waves. The scales for the dependent variables are given by

$$\phi_0 = g Q_0 l/N\Theta_0 \quad , \quad \theta_0 = \Theta_0\phi_0/gH \tag{2.8}$$

$$u_0 = \phi_0/NH \quad , \quad v_0 = a u_0/l \quad , \quad w_0 = H u_0/l \tag{2.9}$$

When these are substituted in the equations and the asterisks dropped the result is

$$\epsilon u + \delta\, \underline{u}.\nabla u - \tfrac{1}{2} y v = -\partial\phi/\partial x \tag{2.10}$$

$$(a/l)^2(\epsilon v + \delta\, \underline{u}.\nabla v) + \tfrac{1}{2} y u = -\partial\phi/\partial y \tag{2.11}$$

$$\epsilon\theta + \delta\, \underline{u}.\nabla\theta + w = Q \tag{2.12}$$

$$\theta = \partial\phi/\partial z \tag{2.13}$$

$$\partial u/\partial x + \partial v/\partial y + \partial w/\partial z = 0 \tag{2.14}$$

where $\epsilon = r l/NH$ and $\delta = \phi_0/N^2H^2 = u_0/c$ (2.15)

Cont/d

The frictional parameter ϵ can be interpreted as the ratio of the given scale ℓ to the Kelvin wave decay distance, c/r. The amplitude or non-linearity parameter δ is the ratio of the particle velocity to the wave velocity.

The above non-dimensional form is appropriate to the heating region only, as the zonal scale has been chosen to equate the zonal extent of this region. The meridional scale is the equatorial Rossby radius. The response to the heating, however, is not confined to the heating region, but is spread out over a region of much greater zonal extent. This can be attributed to the propagation of equatorially trapped waves to both east and west. As they propagate outwards, these waves decay very slowly and so carry information to a large distance inversely proportional to the friction parameter ϵ. The distance is, in fact, of order NH/2 since the wave speed is of order NH.

For the outer region a different non-dimensionalisation is appropriate and the outer variables will be denoted by capital letters. The zonal scale is larger, so the outer zonal distance variable X is given by

$$X = \epsilon x \tag{2.16}$$

The y and z variables are unchanged. The dependent variables u, ϕ and θ are also unchanged since they must match the corresponding inner variables. But the meridional and vertical velocity scales are much smaller in the outer region, so the appropriate non-dimensional variables are

$$V = v/\epsilon \quad , \quad W = w/\epsilon \tag{2.17}$$

The equations for the outer (frictional decay) region, therefore, are

$$u + \delta \underline{u} \cdot \nabla u - \tfrac{1}{2} y V = -\partial\phi/\partial X \tag{2.18}$$

$$(\epsilon a/\ell)^2 (V + \delta \underline{u} \cdot \nabla V) + \tfrac{1}{2} y u = -\partial\phi/\partial y \tag{2.19}$$

$$\theta + \delta \underline{u} \cdot \nabla\theta + W = 0 \tag{2.20}$$

$$\theta = \partial\phi/\partial z \tag{2.21}$$

$$\partial u/\partial X + \partial V/\partial y + \partial W/\partial z = 0 \tag{2.22}$$

The configuration of the inner and outer regions is shown in figure 1.

Cont/d

3. Linear solution in the heating (inner) region

The linear solution corresponds to $\delta = 0$, and in the small-friction limit ($\epsilon \to 0, \epsilon(a/\ell)^2 \to 0$) equations (2.10) - (2.14) reduce to

$$-\tfrac{1}{2} y v = -\partial\phi/\partial x \quad , \quad \tfrac{1}{2} y u = -\partial\phi/\partial y \tag{3.1}$$

$$w = Q \quad , \quad \theta = \partial\phi/\partial z \tag{3.2}$$

$$\partial u/\partial x + \partial v/\partial y + \partial w/\partial z = 0 \tag{3.3}$$

In other words the motion is geostrophic, hydrostatic, and incompressible with w equal to the prescribed heating function. Thus the linear frictionless solution has very simple dynamics.

Following Gill (1980), the vertical structure is given a very simple form in order to simplify the mathematics. It is assumed that the flow is confined between two rigid horizontal planes, one at $z = 0$ and the other (representing the tropopause) a distance πH above, where H is given a value of 4km. The forcing function is assumed to vary sinusoidally with height, so that the solution has the form

$$\theta = \theta_1 \sin z \quad , \quad w = w_1 \sin z \quad , \quad Q = Q_1 \sin z \tag{3.4}$$

$$u = u_1 \cos z \quad , \quad v = v_1 \cos z \quad , \quad \phi = \phi_1 \cos z \tag{3.5}$$

Thus if the heating is strongest at mid-height, in accordance with (3.4), the response in temperature and vertical velocity is also largest at mid-height. However, the horizontal velocity and pressure responses are largest at the surface and at the tropopause. With the above substitution (3.1) to (3.3) reduce to

$$-\tfrac{1}{2} y v_1 = -\partial\phi_1/\partial x \quad , \quad \tfrac{1}{2} y u_1 = -\partial\phi_1/\partial y \tag{3.6}$$

$$w_1 = Q_1 \quad , \quad \theta_1 = -\phi_1 \tag{3.7}$$

$$\partial u_1/\partial x + \partial v_1/\partial y + w_1 = 0 \tag{3.8}$$

It is useful to add to these the vorticity equation obtained by eliminating ϕ, from (3.6) and then substituting from (3.8) for the divergence. The result is

$$v_1 = y w_1 = y Q_1 \tag{3.9}$$

where (3.7) has been used to substitute for w_1. Thus not only is the vertical velocity determined directly by the heating, but so is the

Cont/d

meridional velocity. For positive Q_1 (heating), w is everywhere positive (hot air rises), so stretching vortex lines in the lower atmosphere. As a consequence, the vorticity equation requires poleward motion throughout the lower layer in the heating region.

As for the other variables, it can be seen that these are determined up to an arbitrary function of y since, given v, and w, (3.6) gives $\partial \phi_1/\partial x$, and (3.8) gives $2u_1/\partial x$. The arbitrary function can only be determined by matching with the outer solution, which means taking account of the wave dynamics.

To fix ideas, consider the case where the heating is confined to the region $0<x<1$, where it has the form (cf. Gill 1980)

$$Q_1 = \sin \pi x \, D_0(y) \tag{3.10}$$

where $$D_0(y) = \exp\left(-\tfrac{1}{4}y^2\right) \tag{3.11}$$

is the parabolic cylinder function of order zero (Abramowitz and Stegun 1965). It follows from (3.7) and (3.9) that

$$w_1 = \sin \pi x \, D_0(y) \tag{3.12}$$

$$v_1 = \sin \pi x \, y \exp\left(-\tfrac{1}{4}y^2\right) = \sin \pi x \, D_1(y) \tag{3.13}$$

We can now find ϕ, by integrating the first of equations (3.1) and applying radiation conditions at both the eastern and western boundaries of the heating region. The condition at the eastern boundary $x = 1$ is that only Kelvin waves can be radiated from here, so the meridional structure must be that of a Kelvin wave, namely

$$\phi_1 = A \exp\left(-\tfrac{1}{4}y^2\right) = A D_0(y) \quad \text{at} \quad x = 1 \tag{3.14}$$

The constant A is the amplitude of the radiated Kelvin wave.

The integral of (3.6) satisfying the condition (3.14) is

$$\phi_1 = -\frac{1}{2\pi}(1+\cos \pi x)\, y^2 D_0(y) + A D_0(y) \tag{3.15}$$

The corresponding u_1 field follows from the second of equations (3.6) namely the geostrophic equation, and has the form

$$u_1 = \frac{1}{2\pi}(1+\cos \pi x)(4-y^2) D_0(y) + A D_0(y) \tag{3.16}$$

Cont/d

It follows that the variable q_1, defined below, is given by

$$q_1 = \phi_1 + u_1 = \frac{1}{\pi}(1+\cos\pi x)(2-y^2)D_0(y) + 2A D_0(y)$$
$$= \frac{1}{\pi}(1+\cos\pi x)\left(D_0(y) - D_2(y)\right) + 2A D_0(y) \qquad (3.17)$$

Now the radiation condition at the western boundary $x = 0$ of the heating region can be applied. Here the Kelvin wave amplitude must be zero as no waves can come from the west. This condition is that the projection of q_1, on $D_0(y)$ at $x = 0$ must be zero, i.e.

$$2/\pi + 2A = 0 \quad \Rightarrow \quad A = -1/\pi \qquad (3.18)$$

The values on the western boundary $x = 0$ are

$$\phi_1 = \frac{-1}{\pi}(y^2+1)\exp(-\tfrac{1}{4}y^2) \quad , \quad u_1 = \frac{1}{\pi}(3-y^2)\exp(-\tfrac{1}{4}y^2) \qquad (3.19)$$

The complete inner solution is displayed in figure 2.

Now consider the remaining physical implications. Because the low level flow is poleward, the geostrophic relation (first of 3.6) for ϕ, shows that the surface pressure is low towards the west. The lowest pressures are found on the western edge of the heating region. The minimum will be where $\partial\phi_1/\partial y$ is zero, i.e. (second of 3.6) where u_1 vanishes. This is at $y^2 = 3$ by the second of (3.19), so by the first of (3.19)

$$\min \phi_1 = -\frac{4}{\pi}\exp(-3/4) = -0.6 \quad \text{at } x=0,\ y=\pm 1.73 \qquad (3.20)$$

The flow itself is exactly geostrophic and so is along pressure contours. The strongest inflow is on the equator at the western boundary where by (3.19)

$$\max u_1 = 3/\pi \quad \text{at } x=0,\ y=0 \qquad (3.21)$$

The flow along the equator decelerates with downstream distance in order to provide the rate of convergence given by (3.7), (3.8), and (3.9), i.e.

$$\partial u_1/\partial x = -2Q_1 \qquad (3.22)$$

The value of u_1 on the equator is given (from 3.16 and 3.18) by

Cont/d

$$u_1 = (1 + 2\cos\pi x)/\pi \qquad \text{on } y = 0 \tag{3.23}$$

So the flow reaches a stagnation point at $x = 2/3$, two thirds of the way across the heating region. The configuration of the streamlines $\phi_1 = -1/\pi$ which pass through the stagnation point can be seen in figure 2. One line is the equator along which the flow converges towards the stagnation point. Then the flow diverges meridionally from the stagnation point and curves towards the west. Another interesting result is that the inflow at the equator at the eastern boundary $x = 1$ is given by

$$u_1 = -1/\pi \qquad \text{at } x = 0,\ y = 0 \tag{3.24}$$

and so is only one third as strong as the inflow from the west.

4. Linear solution in the wave decay (outer) regions

The linear equations for the outer regions are (2.18) - (2.22) with $\delta = 0$. Also, in the small friction limit, it has already been assumed that ϵ and $\epsilon(a/\ell)^2$ are vanishingly small, so their product $(\epsilon a/\ell)^2$ is also vanishingly small. The appropriate equations are therefore

$$u - \tfrac{1}{2} y V = -\partial\phi/\partial x \tag{4.1}$$
$$\tfrac{1}{2} y u = -\partial\phi/\partial y \tag{4.2}$$
$$\Theta + W = 0\,, \quad \Theta = \partial\phi/\partial z \tag{4.3}$$
$$\partial u/\partial x + \partial V/\partial y + \partial W/\partial z = 0 \tag{4.4}$$

As no forcing terms appear in these equations (they only apply outside the heating region), the solutions are determined entirely by matching with the inner region. The matching is straightforward, because the fact that the outer regions support decaying equatorially trapped waves has already been exploited by applying radiation conditions to the inner region and getting the complete solution there.

The vertical structure is determined by the matching, and so has the same from as (3.4) and (3.5). Hence (4.1) to (4.4) become

$$u_1 - \tfrac{1}{2} y V_1 = -\partial\phi_1/\partial x \tag{4.5}$$
$$\tfrac{1}{2} y u_1 = -\partial\phi_1/\partial y \tag{4.6}$$
$$\phi_1 = -\Theta_1 = W_1 \tag{4.7}$$
$$\partial u_1/\partial x + \partial V_1/\partial y + \phi_1 = 0 \tag{4.8}$$

Cont/d

The vorticity equation in this case is obtained by adding the y-derivative of (4.5) minus the x - derivative of (4.6) and $\frac{1}{2}y$ times (4.8). The result is

$$\partial u_1/\partial y + \tfrac{1}{2} y \phi_1 - \tfrac{1}{2} V_1 = 0 \qquad (4.9)$$

However, the most useful form of equations (4.5) to (4.8) is obtained by expressing them in terms of the new dependent variables (Gill and Clarke 1974)

$$q_1 = \phi_1 + u_1 \quad , \quad r_1 = \phi_1 - u_1 \qquad (4.10)$$

The three equations below are, firstly, the sum and difference of (4.5) and (4.8), and then (4.6)

$$\partial q_1/\partial x + q_1 + \partial V_1/\partial y - \tfrac{1}{2} y V_1 = 0 \qquad (4.11)$$

$$-\partial r_1/\partial x + r_1 + \partial V_1/\partial y + \tfrac{1}{2} y V_1 = 0 \qquad (4.12)$$

$$\partial q_1/\partial y + \tfrac{1}{2} y q_1 = -\partial r_1/\partial y + \tfrac{1}{2} y r_1 \qquad (4.13)$$

These equations involve the index-raising and index-lowering operations for the parabolic cylinder function $D_n(y)$ (Abramowitz and Stegun 1965), i.e. these functions have the property

$$d D_n/d y + \tfrac{1}{2} y D_n = n D_{n-1} \qquad (4.14)$$

$$d D_n/d y - \tfrac{1}{2} y D_n = - D_{n+1} \qquad (4.15)$$

It follows that if q_1 and r_1 are expanded in these functions e.g.

$$q_1 = \sum_{n=0}^{\infty} q'_n(x)\, D_n(y) \qquad (4.16)$$

equations (4.11) to (4.13) reduce to

$$q'_1 = 0 \qquad (4.17)$$

$$\partial q'_0/\partial x + q'_0 = 0 \qquad (4.18)$$

$$\left.\begin{aligned} (n+1) q'_{n+1} &= r'_{n-1} \\ \partial q'_{n+1}/\partial x + q'_{n+1} &= V'_n \\ \partial r'_{n-1}/\partial x - r'_{n-1} &= n V'_n \end{aligned}\right\} \quad n \geq 1 \qquad (4.19)$$

Elimination of V'_n and r'_{n-1} from (4.19) gives

$$\partial q'_{n+1}/\partial x - (2n+1) q'_{n+1} = 0 \qquad n \geq 1 \qquad (4.20)$$

Now consider the matching condition at the boundaries $x = 0$ and $x = 1$

Cont/d

of the forcing region, which are equivalent in the stretched variables to $X = 0-$ and $X = 0+$ respectively. At the eastern boundary (3.17) and (3.18) give

$$q_1 = -\frac{2}{\pi} D_0(y) \quad \text{at } X = 0+ \tag{4.21}$$

while at the western boundary

$$q_1 = -\frac{2}{\pi} D_2(y) \quad \text{at } X = 0- \tag{4.22}$$

It follows that in the eastern wave region the only non-zero coefficient in (4.16) is q_0' (as the radiation condition required), and hence from (4.18) and (4.21) that

$$\left.\begin{aligned} q_0' &= -2/\pi \exp(-X) \\ q_1 &= -\frac{2}{\pi} D_0(y) \exp(-X) \end{aligned}\right\} \tag{4.23}$$

This decays eastward as required, and represents a decaying Kelvin wave. For such a wave V_1 and λ_1 are zero (e.g. by 4.11 to 4.13) so u_1 and ϕ_1 are given by

$$u_1 = \phi_1 = -\frac{1}{\pi} D_0(y) \exp(-X) \quad \text{for } X > 0 \tag{4.24}$$

Now consider the western wave region. The coefficient q_0' is zero here as required by the radiation condition. Moreover, (4.22) shows that all the other coefficients q_n' vanish with the exception of q_2'. From (4.20) and (4.22) this is given by

$$\left.\begin{aligned} q_2' &= -\frac{2}{\pi} \exp(3X) \\ q_1 &= -\frac{2}{\pi} D_2(y) \exp(3X) \end{aligned}\right\} \tag{4.25}$$

The only non-zero coefficients in the expressions of λ_1 and V_1 are

$$\begin{aligned} \lambda_0' &= 2q_2' = -\frac{4}{\pi} \exp(3X) \\ V_1' &= 4q_2' = -\frac{8}{\pi} \exp(3X) \end{aligned} \tag{4.26}$$

by (4.19). Hence (4.10) gives

$$\left.\begin{aligned} \phi_1 &= -\frac{1}{\pi}(y^2+1) \exp(3X - \tfrac{1}{4}y^2) \\ u_1 &= -\frac{1}{\pi}(y^2-3) \exp(3X - \tfrac{1}{4}y^2) \\ V_1 &= -\frac{8}{\pi} y \exp(3X - \tfrac{1}{4}y^2) \end{aligned}\right\} \quad X < 0 \tag{4.27}$$

Cont/d

This represents the slowest decaying planetary wave mode. The complete outer solution, given by (4.24) and (4.27) is shown in figure 3. The heating region is a line singularity at $X = 0$.

Two of the most striking features of the solution are that the decay rate is three times larger in the western region than in the eastern region, and that the inflow into the heating region along the equator is again three times larger in the western region than in the eastern regio These results are intimately related, and can be explained without going through the detailed calculations.

Consider first the ratio of the decay rates. The Rayleigh friction and Newtonian cooling provide a time decay rate proportional to r and the amplitude. Therefore the spatial decay rate will be proportional to r and the amplitude, but inversely proportional to the propagation rate of the waves. The propagation rate is the group velocity, which fo the eastward propagating Kelvin wave is $c=NH$. The group velocity for the fastest westward propagating wave, the lowest mode planetary wave, is $-c/3$, only one third of the Kelvin wave speed. The decay rate of the waves on the western side will therefore be three or more times larger than on the eastern side.

Consider now the ratio of the inflow magnitudes. At the equator we see from (4.1) that in the wave decay regions there is a frictional balance between the Rayleigh friction term and the pressure gradient in the direction of the flow, namely

$$\partial\phi/\partial X = -u \qquad \text{on } y=0 \tag{4.28}$$

Moreover, the pressure drop across the heating region is negligibly small in the low friction limit, as expressed mathematically by (3.1)

$$\partial\phi/\partial x = 0 \qquad \text{on } y=0,\ 0<x<1 \tag{4.29}$$

Consequently the pressure drop across the two wave regions is the same and, integrating (4.28), we find that $\int u\,dX$ along the equator must be equal and opposite in the two decay regions. But since the velocity decays exponentially in both regions, and since the decay rate is three times larger in the western region than in the eastern region, we conclude that the amplitude in the western region must also be three times larger.

Cont/d

5. Total vorticity field

A useful field for the analysis of the atmospheric circulation is the total vorticity . For instance, Sardeshmukh and Hoskins (1985) have studied this field in the tropics in connection with the 1982-83 El Niño-Southern Oscillation event. Consider the form this quantity takes. In terms of dimensional quantities, it is given by

$$f + \zeta = \beta y + \partial v/\partial x - \partial u/\partial y \qquad (5.1)$$

The appropriate non-dimensional scale for f is $2\beta a$ while the non-dimensional form ζ for the relative vorticity is given by

$$\zeta_* = \zeta a/u_0 \qquad (5.2)$$

Thus, after dropping asterisks, the non-dimensional total vorticity is given by

$$\tfrac{1}{2}y + \delta\zeta = \tfrac{1}{2}y + \delta\left(-\partial u/\partial y + (a/\ell)^2 \partial v/\partial x\right) \qquad (5.3)$$

or, alternatively using outer region scales

$$\tfrac{1}{2}y + \delta\zeta = \tfrac{1}{2}y + \delta\left(-\partial u/\partial y + (\epsilon a/\ell)^2 \partial V/\partial X\right) \qquad (5.4)$$

The vertical structure for ζ is the same as for horizontal velocity, namely

$$\zeta = \zeta_1 \cos z \qquad (5.5)$$

For the inner region, in the limit of small (a/ℓ), the total vorticity can be calculated from (5.3), (5.5), (3.13), (3.16) and (3.18). These equations give

$$\tfrac{1}{2}y + \delta\zeta = \tfrac{1}{2}y\left\{1 + \frac{\delta}{\pi}\cos z\left[(3 - \tfrac{1}{2}y^2) + \cos\pi x\,(4 - \tfrac{1}{2}y^2)\right]\exp\left(-\tfrac{1}{4}y^2\right)\right\} \qquad (5.6)$$

This field is shown in figure 4 at both (a) the surface $z = 0$ and (b) the tropopause $z = \pi$. The dominant feature is the pinching together of contours at the lower level and spreading apart at the upper level, the maximum effect being at the western edge $x = 0$ of the forcing region where

$$\tfrac{1}{2}y + \delta\zeta = \tfrac{1}{2}y\left[1 + \frac{\delta}{\pi}\cos z\,(7 - y^2)\exp\left(-\tfrac{1}{4}y^2\right)\right] \quad \text{at } x = 0 \qquad (5.7)$$

Cont/d

The graphs are drawn for the value at which the vorticity gradient first attains a zero value, at $x=0, y=0$ when

$$\delta = \pi/7 \simeq 0.45 \quad \text{, for small } (a/\ell) \qquad (5.8)$$

Patterns with the total vorticity contours spread apart by this amount do occur at 200mb. If N is $10^{-2}s^{-1}$ and H is 4km, NH is 40 ms^{-1} so this value of δ corresponds to a maximum velocity of

$$3\delta NH/\pi = 120/7 \ ms^{-1} \simeq 17 \ ms^{-1}$$

Note that the apparently non-linear total vorticity field is obtained using only the linear solution, as this gives the field correct to order δ. No account has yet been made of non-linear self-interaction which will be discussed in the remaining sections.

It is appropriate at this point to explain how the diagram like figure 4 which show both inner and outer regions are constructed, because the geometry chosen to display the information appears to imply that certain finite values of a/ℓ and ϵ are chosen. The implied values in figure 4 are π^{-1} and 0.2, respectively, since the diagram is drawn with the same zonal and meridional scales according to normal practice. The scales marked are in units of the equatorial Rossby radius a and the heating region is in the range $0 \leq x \leq \pi$. The solution depicted, however, is calculated as explained in the text i.e. for the limit of vanishing ϵ and, a/ℓ, and its representation using a geometry appropriate to small but finite values of ϵ and a/ℓ is purely a matter of convenience. In this sense they differ from the diagram shown in Gill (1980) which were calculated for small but finite ϵ and a/ℓ. The reason for choosing the limiting case in this study is to emphasize the effects of non-linearity when friction is very weak, the idea being that if some effects normally attributed to friction could in fact be due to non-linearity, this would be revealed in such a study.

6. Non-linear Modifications

The linear solution discussed in the previous section can be regarded as the first term in an expansion in power of δ, the amplitude parameter and the purpose of the remaining part of this paper is to calculate the first non-linear connection to the linear solution. In other words, if variables are expanded in the form

Cont/d

$$u = u_L + u_{NL} \tag{6.1}$$

where suffix L refers to the linear solution and NL to the non-linear connection, the purpose is to calculate u_{NL} for small value of δ. The equations satisfied by u_{NL}, etc. are easily obtained from those in section 2, e.g. the ones for the inner region for small friction are

$$-\tfrac{1}{2} y v_{NL} = -\partial \phi_{NL}/\partial x + M \tag{6.2}$$

$$w_{NL} = T \quad , \quad \theta_{NL} = \partial \phi_{NL}/\partial z \tag{6.3}$$

$$\tfrac{1}{2} y u_{NL} = -\partial \phi_{NL}/\partial y \quad , \quad \partial u_{NL}/\partial x + \partial v_{NL}/\partial y + \partial w_{NL}/\partial z = 0 \tag{6.4}$$

where M will be called the mechanical forcing term due to non-linear self-interactions in the linear solution, and T will be called the thermal forcing term. There is also another forcing term of order $(a/\ell)^2$ but for simplicity this will not be calculated, on the grounds that (a/ℓ) is often small. The forcing terms M and T are given by

$$-M = u_L \partial u_L/\partial x + v_L \partial u_L/\partial y + w_L \partial u_L/\partial z \tag{6.5}$$

$$-T = u_L \partial \theta_L/\partial x + v_L \partial \theta_L/\partial y + w_L \partial \theta_L/\partial z \tag{6.6}$$

Note that the vertical velocity w_{n2} is completely determined by the linear solution in the same way that w_2 was determined by the heating function.

The vorticity equation can be obtained from (6.2) and (6.4) in the same way as (3.9) was derived. The result is

$$\begin{aligned} v_{NL} &= y \partial u_{NL}/\partial z - 2 \partial M/\partial y \\ &= y \partial T/\partial z - 2 \partial M/\partial y \end{aligned} \tag{6.7}$$

using (6.3). Thus, as for the linear case, the meridional velocity v_{NL} is also completely determined from knowledge of the linear solution. Similarly, (6.2) and (6.4) show that the x-gradient of ϕ_{NL} and u_{NL} are determined, but the actual values of the fields can only be obtained by integrating with respect to x and applying matching conditions at the eastern and western boundaries.

The equations for the outer regions follow from (2.18) to (2.22) and take the form

Cont/d

$$u_{NL} - \tfrac{1}{2} V_{NL} = -\partial \phi_{NL}/\partial X + M \qquad (6.8)$$

$$\theta_{NL} + W_{NL} = T \quad , \quad \theta_{NL} = \partial \phi_{NL}/\partial z \qquad (6.9)$$

$$\tfrac{1}{2} u_{NL} = -\partial \phi_{NL}/\partial y \quad , \quad \partial u_{NL}/\partial X + \partial V_{NL}/\partial y + \partial W_{NL}/\partial z = 0 \qquad (6.10)$$

where M and T are given by

$$-M = u_L \partial u_L/\partial X + V_L \partial u_L/\partial y + W_L \partial u_L/\partial z \qquad (6.11)$$

$$-T = u_L \partial \theta_L/\partial X + V_L \partial \theta_L/\partial y + W_L \partial \theta_L/\partial z \qquad (6.12)$$

Again the forcing is by known functions M and T, the only difference from the inner region being the appearance of the friction and cooling terms in (6.8) and (6.9).

Now consider the vertical structure of the forcing terms M and T, which follows from substitution of (3.4) and (3.5) in the expression for M and T. These give

$$M = M_0 + M_2 \cos 2z \quad , \quad T = T_2 \sin 2z \qquad (6.13)$$

where

$$-2M_0 = u_1 \partial u_1/\partial x + v_1 \partial u_1/\partial y - w_1 u_1 \qquad (6.14)$$

$$-2M_2 = u_1 \partial u_1/\partial x + v_1 \partial u_1/\partial y + w_1 u_1 \qquad (6.15)$$

$$-2T_2 = u_1 \partial \theta_1/\partial x + v_1 \partial \theta_1/\partial y + w_1 \theta_1 \qquad (6.16)$$

in the inner region. Similar expressions with capital X, V and W apply in the outer regions. Note that the expression for T_2 can be simplified. For the inner region the first two terms cancel each other by the geostrophic relation (3.6) and the hydrostatic equation (3.7), and so

$$T_2 = -\tfrac{1}{2} G_1 \theta_1 \qquad (6.17)$$

For the outer region a similar substitution from (4.5) to (4.7) gives

$$T_2 = -\tfrac{1}{2} \left(u_1^2 - \theta_1^2 \right) \qquad (6.18)$$

From the above it follows that there is a depth independent mechanical forcing term which will generate a depth-independent (barotropic) response. The terms M_2 and T_2 generate a second baroclinic mode with a full wave in the vertical, rather than half a wave as for the linear solution. Thus the dependent variables for the non-linear correction have the form

$$u_{NL} = u_0 + u_2 \cos 2z \quad , \quad v_{NL} = v_0 + v_2 \cos 2z \quad , \quad \phi_{NL} = \phi_0 + \phi_2 \cos 2z \qquad (6.19)$$

Cont/d

$$w_{NL} = w_2 \sin 2z \quad , \quad \theta_{NL} = \theta_2 \sin 2z \tag{6.20}$$

The next two sections deal with the barotropic and the second baroclinic modes explicitly, and the necessary analytic results are derived. Discussion of the dynamics will be left to a later section.

7. The Barotropic component

The barotropic part of the flow is driven by the mechanical forcing term M, which is given by (6.14). In the inner region, substitution from (3.12), (3.13), (3.16) and (3.18) gives

$$M_0 = \frac{1}{4\pi}\left[(6-y^2)+(12-y^2)\cos\pi x\right]\sin\pi x \exp\left(-\tfrac{1}{2}y^2\right) \tag{7.1}$$

The equations for the inner region follow from substitution of (6.13) and (6.19) in (6.2) to (6.4), which gives

$$-\tfrac{1}{2} y v_0 = -\partial\phi_0/\partial x + M_0 \tag{7.2}$$

$$\tfrac{1}{2} y u_0 = -\partial\phi_0/\partial y \tag{7.3}$$

$$\partial u_0/\partial x + \partial v_0/\partial y = 0 \tag{7.4}$$

while the vorticity equation (6.7) yields the meridional velocity explicitly,

$$v_0 = -2\frac{\partial M_0}{\partial y} = \frac{1}{2\pi}\left[(8-y^2)+(14-y^2)\cos\pi x\right]\sin\pi x \; y \exp\left(-\tfrac{1}{2}y^2\right) \tag{7.5}$$

The geopotential ϕ, follows by integrating (7.2), namely

$$\phi_0 = -\frac{1}{16\pi^2}\Big[4(1+\cos\pi x)(6+7y^2-y^4) - (1-\cos 2\pi x)(12+13y^2-y^4)\Big]\exp\left(-\tfrac{1}{2}y^2\right) + A(y) \tag{7.6}$$

where $A(y)$ is the value on the eastern boundary, which has yet to be determined. The corresponding u_0 follows from geostrophy, i.e. equation (7.3), and is given by

$$u_0 = \frac{1}{8\pi^2}\Big[4(1+\cos\pi x)(-8+11y^2-y^4) - (1-\cos 2\pi x)(-14+17y^2-y^4)\Big]\exp\left(-\tfrac{1}{2}y^2\right) - \frac{2}{y}\frac{dA}{dy} \tag{7.7}$$

Now consider the barotropic flow in the outer regions. The equations obtained from substitution of (6.13) and (6.19) in (6.8) and (6.10) are

Cont/d

$$u_0 - \tfrac{1}{2} y V_0 = -\partial \phi_0 / \partial X + M_0 \qquad (7.8)$$

$$\tfrac{1}{2} y u_0 = -\partial \phi_0 / \partial y \qquad (7.9)$$

$$\partial u_0 / \partial X + \partial V_0 / \partial y = 0 \qquad (7.10)$$

The vorticity equation obtained by subtracting the X derivative of (7.9) from the y derivative of (7.8) and using (7.10) is

$$\partial u_0 / \partial y - \tfrac{1}{2} V_0 = \partial M_0 / \partial y \qquad (7.11)$$

Taking minus the X-derivative and using (7.10) gives

$$\partial^2 V_0 / \partial y^2 + \tfrac{1}{2} \partial V_0 / \partial X = \partial^2 M_0 / \partial X \partial y \qquad (7.12)$$

This equation applies in both outer regions, but they must be dealt with separately. First consider the eastern region where V_1 is zero, and substitution of (4.24) and (4.7) in (6.14) gives

$$M_0 = -\frac{1}{2}\left(u_1 \partial u_1 / \partial X - W_1 u_1\right) = u_1^2 = \frac{1}{\pi^2} \exp\left(-2X - \tfrac{1}{2} y^2\right) \qquad (7.13)$$

The solution of (7.12) which decays at $X=\infty$ has the form

$$V_0 = G(y) \exp(-2X) \qquad (7.14)$$

where $$d^2 G / d y^2 - G = -\frac{2}{\pi^2} y \exp\left(-\tfrac{1}{2} y^2\right) \qquad (7.15)$$

The solution of (7.15) can be obtained explicitly by standard methods, and has the form

$$G = \left(\frac{e}{2\pi^3}\right)^{1/2} \left\{ e^{y} \left[\operatorname{erf}\left(\frac{y+1}{\sqrt{2}}\right) - 1 \right] + e^{-y} \left[\operatorname{erf}\left(\frac{y-1}{\sqrt{2}}\right) + 1 \right] \right\} \qquad (7.16)$$

where erf is the error function defined as follows

$$\operatorname{erf}(x) = \frac{2}{\sqrt{\pi}} \int_0^x \exp\left(-t^2\right) dt \qquad (7.17)$$

The expression for u_0 follows from (7.9) which gives

$$u_0 = \tfrac{1}{2} d G / d y \; e^{-2X} \qquad (7.18)$$

and from (7.16)

$$dG/dy = \left(\frac{e}{2\pi^3}\right)^{1/2} \left\{ e^{y} \left[\operatorname{erf}\left(\frac{y+1}{\sqrt{2}}\right) - 1 \right] - e^{-y} \left[\operatorname{erf}\left(\frac{y-1}{\sqrt{2}}\right) + 1 \right] \right\} + \frac{2}{\pi^2} \exp\left(-\tfrac{1}{2} y^2\right) \qquad (7.19)$$

Cont/d

The function $A(y)$ in (7.6) and (7.7) now follows from comparing (7.7) and (7.18) at the eastern boundary of the heating region, giving

$$A' = -\frac{1}{4} y\, G' \tag{7.20}$$

This can be integrated to give

$$A(y) = \frac{1}{4}\left(\frac{c}{2\pi^3}\right)^{1/2}\left\{(1-y)e^{y}\left[\mathrm{erf}\left(\frac{y+1}{\sqrt{2}}\right)-1\right] - (1+y)e^{-y}\left[\mathrm{erf}\left(\frac{y-1}{\sqrt{2}}\right)+1\right]\right\} \tag{7.21}$$

and in the eastern region the barotropic pressure is then

$$\phi_0 = A(y)\, e^{-2X} \tag{7.22}$$

Finally, the western decay region must be considered. Here we take the y-derivative of (7.11), and using (7.10), we find

$$\partial^2 u_c/\partial y^2 + \frac{1}{2}\,\partial u_c/\partial X = \partial^2 M_c/\partial y^2 \tag{7.23}$$

where $$M_0 = \frac{-1}{\pi^2}\left(15 + 6y^2 - y^4\right)\exp\left(6X - \frac{1}{2}y^2\right) \tag{7.24}$$

The boundary condition for (7.23) at X=0 is, from (7.7) and (7.18)

$$u_0 = \frac{1}{\pi^2}\left(8 - 11y^2 + y^4\right)\exp\left(-\frac{1}{2}y^2\right) + \frac{1}{2}\,dG/dy \tag{7.25}$$

The solution of (7.23) can be written as an integral equation, but, as this would have to be evaluated numerically, it proves easier to solve (7.23) directly by numerical means. We do this using centered differences in y and forward 'time' (i.e. the -X direction) steps. The barotropic solution so obtained is shown in figure 5(a).

8. The Second Baroclinic mode component

The remaining part of the non-linear correction is in the second baroclinic mode, denoted by the suffix 2, and driven by the terms M_2 and T_2. The equations for the inner region follow from substitution of (6.13), (6.19) and (6.20) in (6.2) to (6.4) and take the form

$$-\frac{1}{2}y\,v_2 = -\partial\phi_2/\partial x + M_2 \tag{8.1}$$

$$w_2 = T_2\ ,\quad \theta_2 = -2\phi_2 \tag{8.2}$$

$$\frac{1}{2}y\,u_2 = -\partial\phi_2/\partial y \tag{8.3}$$

$$\partial u_2/\partial x + \partial v_2/\partial y + 2\,w_2 = 0 \tag{8.4}$$

Cont/d

Similarly, the vorticity equation (6.7) gives

$$v_2 = 2y T_2 - 2\,\partial M_2/\partial y \qquad (8.5)$$

so both w_2 and v_2 are given explicitly by (8.2) and (8.5). The problem is formally the same as for the linear case, the only difference being in the form of the forcing term, and in the fact that the equatorial Rossby radius is smaller by a factor of $\sqrt{2}$. For this reason it is convenient to express solutions in terms of parabolic cylinder functions $E_n(y)$ with the new scale instead of the old one, i.e. defined by

$$E_n(y) = D_n(\sqrt{2}y) \qquad (8.6)$$

The forcing functions follow from substitution of (3.7), (3.10), (3.15) (3.16) and (3.18) in (6.15) and (6.17). The result is

$$M_2 = \frac{1}{4\pi}\left[(2+y^2)+(4+y^2)\cos\pi x\right]\sin\pi x\,\exp(-\tfrac{1}{2}y^2) \qquad (8.7)$$

$$T_2 = \frac{1}{4\pi}\left[(2+y^2)+y^2\cos\pi x\right]\sin\pi x\,\exp(-\tfrac{1}{2}y^2) \qquad (8.8)$$

and so by (8.5)

$$v_2 = \frac{1}{\pi}\sin\pi x\,(\cos\pi x - 1)\,y\,\exp(-\tfrac{1}{2}y^2) \qquad (8.9)$$

The geopotential ϕ_2 can now be obtained by integrating (8.1) with respect to x to give

$$\phi_2 = \frac{1}{4\pi^2}\left[(1+\cos\pi x)(y^2-2) + (1-\cos 2\pi x)\left(\tfrac{3}{4}y^2+1\right)\right]\exp(-\tfrac{1}{2}y^2) + B(y) \qquad (8.10)$$

where B is a function to be determined by matching with the outer solution. The expression for u_2 now follows from (8.3) and (8.10), namely

$$u_2 = \frac{1}{2\pi^2}\left[(1+\cos\pi x)(y^2-4) + (1-\cos 2\pi x)\left(\tfrac{3}{4}y^2-\tfrac{1}{2}\right)\right]\exp(-\tfrac{1}{2}y^2) - \frac{\varepsilon}{y}\frac{dB}{dy} \qquad (8.11)$$

Now consider the baroclinic part of the non-linear correction in the outer regions. The equations obtained by substitution of (6.13), (6.19) and (6.20) in (6.8) to (6.10) are

$$u_2 - \tfrac{1}{2}yV_2 = -\partial\phi_2/\partial X + M_2 \qquad (8.12)$$

$$\tfrac{1}{2}y u_2 = -\partial\phi_2/\partial y \qquad (8.13)$$

$$\Theta_2 + W_2 = T_2\,, \quad \Theta_2 = -2\phi_2 \qquad (8.14)$$

$$\partial u_2/\partial X + \partial V_2/\partial y + 2W_2 = 0 \qquad (8.15)$$

where $$-2M_2 = u_1\,\partial u_1/\partial X + V_1\,\partial u_1/\partial y + W_1 u_1 \qquad (8.16)$$

Cont/d

$$-2T_2 = u_1 \partial\theta_1/\partial x + V_1 \partial\theta_1/\partial y + W_1\theta_1 \qquad (8.17)$$

As when dealing with the linear solution in the outer regions, it is advantageous to introduce new dependent variables

$$q_2 = 2\phi_2 + u_2 \quad , \quad r_2 = 2\phi_2 - u_2 \qquad (8.18)$$

The sum and difference of (8.12) and (8.15) then become, after using (8.14)

$$\partial q_2/\partial x + 2q_2 + \partial V_2/\partial y - yV_2 = 2(M_2 - T_2) \qquad (8.19)$$

$$\partial r_2/\partial x - 2r_2 - \partial V_2/\partial y - yV_2 = 2(M_2 + T_2) \qquad (8.20)$$

while (8.13) gives

$$\partial q_2/\partial y + yq_2 = -\partial r_2/\partial y + yr_2 \qquad (8.21)$$

By analogy with (4.16), variables are now expanded in the form

$$q_2 = \sum_{n=0}^{\infty} q_n^2(x) E_n(y) \qquad (8.22)$$

and the equations which follow after substitution in (8.19) to (8.21) are

$$q_1^2 = 0 \qquad (8.23)$$

$$\partial q_0^2/\partial x + 2q_0^2 = 2(M_0^2 - T_0^2) \qquad (8.24)$$

$$\left.\begin{aligned} (n+1)\,q_{n+1}^2 &= r_{n-1}^2 \\ \partial q_{n+1}^2/\partial x + 2q_{n+1}^2 - \sqrt{2}\,V_n^2 &= 2(M_{n+1}^2 - T_{n+1}^2) \\ \partial r_{n-1}^2/\partial x - 2r_{n-1}^2 + \sqrt{2}\,n V_n^2 &= 2(M_{n-1}^2 + T_{n-1}^2) \end{aligned}\right\} \quad n \geq 1 \qquad (8.25)$$

and hence

$$\partial q_{n+1}^2/\partial x - 2(2n+1)\,q_{n+1}^2 = 2(M_{n-1}^2 + T_{n-1}^2) - 2n(M_{n+1}^2 - T_{n+1}^2) \qquad (8.26)$$

These equations apply in both outer regions, which must be dealt with separately. Consider first the eastern region where V_1 is zero. Substitution of (4.24) in (8.16) and (8.17) shows the forcing terms are identically zero in the eastern region. Since the only wave which decays eastward is the Kelvin wave, the solution is

$$q_n^2 = 0 \quad n \geq 1 \qquad (8.27)$$

$$q_0^2 = 2C e^{-2x} \qquad (8.28)$$

$$\text{i.e. } 2\phi_2 = u_2 = C \exp(-2x - \tfrac{1}{2}y^2) \qquad (8.29)$$

Cont/d

It follows that the function $b(y)$ in (8.10) is given by

$$B(y) = \frac{c}{2} E_0(y) = \frac{c}{2} \exp\left(-\tfrac{1}{2}y^2\right) \tag{8.30}$$

in order for the inner and outer solutions to match at the eastern boundary of the heating region. At the western boundary (8.10), (8.11) and (8.30) give

$$\begin{aligned} \phi_2 &= \left[\frac{1}{\pi^2}\left(\tfrac{1}{2}y^2 - 1\right) + \frac{c}{2}\right] \exp\left(-\tfrac{1}{2}y^2\right) \\ u_2 &= \left[\frac{1}{\pi^2}\left(y^2 - 4\right) + C\right] \exp\left(-\tfrac{1}{2}y^2\right) \\ q_2 &= \left(-\frac{5}{\pi^2} + 2C\right) E_0(y) + \frac{1}{\pi^2} E_2(y) \end{aligned} \tag{8.31}$$

Now consider the western outer region. Here substitution of (4.27) in (8.16) and (8.17) gives

$$\begin{aligned} M_2 &= \frac{1}{\pi^2}\left[-14 E_0(y) - 2 E_2(y)\right] \exp(6X) \\ T_2 &= \frac{1}{\pi^2}\left[-2 E_0(y) + 2 E_2(y)\right] \exp(6X) \end{aligned} \tag{8.32}$$

It follows that (8.24) gives a forced Kelvin wave solution

$$q_0^2 = -\frac{3}{\pi^2} \exp(6X) \tag{8.33}$$

while (8.26) gives

$$\begin{aligned} &\partial q_2^2/\partial X - 6 q_2^2 = -\frac{24}{\pi^2} \exp(6X) \\ \text{i.e.}\quad &q_2^2 = \frac{1}{\pi^2}(1 - 24X) \exp(6X) \end{aligned} \tag{8.34}$$

for the symmetric planetary wave, the constant being chosen to match (8.31). All the remaining planetary waves are identically zero. The value of the constant C can now be determined by comparing (8.31) and (8.33) at the western boundary, giving

$$C = 1/\pi^2 \tag{8.35}$$

This completes the determination of the baroclinic second mode, which is depicted in figure 5(b). This also completes the determination of the flow field to order δ. Figure 6(b) shows the flow at the surface $z = 0$ for $\delta = 0.45$ for comparison with the linear solution $\delta = 0$ shown in figure 6(a). Figure 7(a) and (b) are the corresponding diagrams for the tropopause $z = \pi$ and figures 7(c) and (d), show the comparison of u contours. The method of constructing diagrams is as outlined in section 5. The value of δ chosen is quite large, for otherwise the

Cont/d

difference made by the non-linearity would be hard to see. The value corresponds to a maximum velocity which is 43% of the wave speed and makes the gradient of absolute vorticity zero at the point of maximum velocity. The main effects that can be discerned in figures 6 and 7 however are that the twin cyclones at the ground are more intense and the westerly jet between them is stronger. At the tropopause the easterly outflow is reduced in strength by the non-linearity, but the effect on the geopotential is better described as a distortion than a noticeable change in the extreme values.

9. Discussion of non-linear effects

Before discussing these effects, it is useful to recall simplifying features of the analysis. One was the neglect of the meridional acceleration term $\underset{\sim}{v}.\nabla v$ which is justified asymptotically in the small friction limit for the outer regions, but requires the aspect ratio a/ℓ to be small to be justified in the inner region. On top of this, numerical circumstances add further simplifications because both winds and their zonal gradients are much larger at the western end of the heating region than at the east. The result is that non-linear corrections are only significant near the western end of the heating region and the decay region immediately to the west. This is clear from the display of the non-linear correction terms in figure 5.

The non-linear effects may be considered in the same order we used to build up the linear solution, that is, first the heat equation and the vertical velocity, then the vorticity equation and the meridional velocity, and finally the zonal velocity and the pressure. In the inner (heating) region, the horizontal advection terms in the heat equation vanish identically because the horizontal flow is along geopotential contours, which coincide with temperature contours at the same level. Therefore (2.12) in the heating region reduces to

$$-(1+\delta\,\partial\Theta/\partial z)w = Q \qquad (9.1)$$

Thus the only non-linear modification is due to the term N^2 which multiplies w in the dimensional equivalent of (9.1). Since the atmosphere is warmed at mid-level, stability and N^2 are reduced in the upper troposphere and increased in the lower troposphere. Consequently the maximum vertical velocity is displaced above the level of maximum heating as shown in figure 8. The divergence at upper levels is increased, and the low level convergence decreased relative to the linear solution. (The divergence at the upper level

Cont/d

is shown in figure 9).

Next we consider the vorticity equation in the heating region, where friction and cooling may be neglected, and we assume a/ℓ is small as well. For simplicity we consider the upper and lower boundaries where w vanishes. Then elimination of ϕ between (2.10) and (2.11) gives the vorticity equation

$$\underline{u}_H \cdot \nabla\left(\tfrac{1}{2} y + \delta\zeta\right) = -\left(\tfrac{1}{2} y + \delta\zeta\right) \nabla \cdot \underline{u}_H \qquad (9.2)$$

$$\zeta = -\partial u / \partial y \qquad (9.3)$$

i.e. the flow across vorticity contours is proportional to the product of vorticity and divergence, and inversely proportional to the vorticity gradient. In the linear case vorticity reduces to planetary vorticity, so that (9.2) reduces to

$$\tfrac{1}{2} v = \tfrac{1}{2} y \, \partial w / \partial z \qquad (9.4)$$

and the divergence is known from the heating (9.1). So the vorticity equation reduces to an equation for the meridional velocity.

For any finite heating strength the vorticity and divergence will not be as in (9.4). However, the modification to the divergence can be estimated from the linear solution using (9.1), and the relative vorticity ζ is also obtained from the linear solution. The total vorticity has been displayed already in figure 4 and its product with the divergence is shown in figure 9. We note, that as we go from the linear to the non-linear case, the largest changes both in vorticity and divergence occur near the equator, where the total vorticity is small. These changes therefore have little effect on the product of vorticity and divergence which is

Cont/d

largest in the regions $1<|y|<2$. For a qualitative explanation of the non-linear vorticity balance (9.2) we may therefore take the right-hand side of (9.2) to be virtually unchanged from linear theory. Then (9.2) requires the flow normal to the absolute vorticity contours times the vorticity gradient to be the same. It can be seen indeed that where the vorticity contours are most distorted in figure 4, so the flow direction (see figure 9) is most distorted as well in order for (9.2) to remain true.

Another useful insight into the effects of non-linearity comes from a consideration of the streamwise balance of momentum on the equator. In the inner region (2.10) reduces to

$$\delta(u\,\partial u/\partial x + w\,\partial u/\partial z) = -\partial\phi/\partial x \qquad (9.5)$$

At the upper and lower boundaries this further reduces to

$$\left.\begin{aligned} &\delta u\,\partial u/\partial x + \partial\phi/\partial x = 0 \\ &\delta \tfrac{1}{2}u^2 + \phi = \text{const.} \end{aligned}\right\} \text{ on } y=0,\ z=0,\pi \qquad (9.6)$$

Thus instead of ϕ being constant, as in the linear case, the total head is constant as given by (9.6). In the linear model the pressure is constant in the inner region at the equator because the velocities are so small that particle acceleration is negligible, and therefore no pressure gradient is required to accelerate them. It follows from the expansion procedure that in the non-linear case there is a pressure drop of $\delta\frac{1}{2}u^2$, being a maximum of $9\delta/2\pi^2$ at the western end of the inner region, zero at the stagnation point, and $\delta/2\pi^2$ at the eastern end of the heating region, as shown in figure 10.

Cont/d

The effect at the surface can be seen in figure 10(a). In the linear case the pressure is everywhere below zero, and is even further reduced in the non-linear case. The lowest pressure is still at the cyclone centre at the western edge of the heating zone, the centre being shifted slightly closer to the equator by the non-linear effect (figure 11(c)). At the upper boundary (figure 11(a)) the pressure is positive everywhere in the linear case, so the Bernoulli effect will reduce this near the equator. The anticyclone centre is shifted slightly away from the equator by the non-linear effects (figure 11(b)). The broadening effect on the easterly outflow is also clear from a comparison of figures 11(a) and 11(b).

The small amplitude expansion technique seems to be a reasonable and practical way of estimating non-linear effects in practice since the general effect appears to be a modest distortion of the flow even for quite large values of the expansion parameter. The only indication of non-linear effects which might not be weak came in the analysis of the total vorticity in section 5 where it was found that the meridional gradient of absolute vorticity changed from its planetary value, beta, to zero at the western end of the heating region at the tropopause when δ attained the value of 0.45. At least, that was the case at order δ. With the non-linear calculations, the total vorticity is now available at order δ^2 so it is of some interest to compare the field at this order with that at order δ. The order δ^2 result at the tropopause level is shown in figure 4(d) so to be adjacent to the order δ result. The gradient is no longer zero anywhere for δ = 0.45, a result which could be anticipated from figure 11b(ii) since the relative vorticity gradient $\partial^2 u/\partial y^2$ is much reduced by the non-linearity at the point in question. There is a certain lack of smoothness which indicates that several terms are needed to give accurate results in this neighbourhood, but the general character is not likely to be different even for δ as high is 0.45.

10. Relation to other work

A problem very similar to the one considered in this paper was studied by means of a primitive equations numerical model by Nobre (1983). One of the cases he studied was that of a single equatorial heat source on a sphere. Nobre chose realistic heating rates, but, in order to reduce the number of zonal harmonics needed in the spectral method of solution, he chose the longitudinal extent of the heating region to be 180°. But from (2.8) and (2.9) we know that u_0 is proportional to $Q\ell$, so that choosing a very large heating region produces very strong winds: the values chosen by Nobre correspond approximately to $\delta = 0.2, 0.4$ and 0.6.

The large heating region and small friction parameter chosen by Nobre result in his Kelvin and planetary waves overlapping, because the flow reaches all the way around the sphere. This makes a quantitative comparison with our results difficult, but this was partially overcome by superposing an array of sources in the form

$$\phi(x+12, y) + \phi(x+6, y) + \phi(x, y) + \phi(x-6, y)$$

to reproduce the effect of periodicity. Figure 12 shows the resulting patterns at the upper and lower boundaries, which are very similar to those obtained by Nobre, even though the averaging technique is not strictly valid for the non-linear case. In both our case and Nobre's, we find the following changes relative to the linear solution:

- more divergence at the upper boundary, and less convergence at the lower boundary,
- the meridional velocity in the heating region shifted east at the upper boundary, west at the lower boundary,
- on the western side of the heating region the easterlies at the upper boundary are weaker, and the westerlies at the lower boundary are stronger,

- on the western side of the heating region the low pressure tongue at the upper boundary extends further east, whilst the high pressure tongue at the lower boundary does not extend as far east.

Nobre also examined the importance of the different terms in the equations, and found that the non-linear terms in the y momentum equation were not important. This we found from the scaling of the equation, (2.11) and (2.19). Finally, we note that as Nobre increased the heating to $\delta = 0.4$ and $\delta = 0.6$ there were no dramatic changes in the flow, just a gradual distortion of the features observed in the linear solution.

Vorticity balances in the tropics have been examined by Sardeshmukh and Hoskins (1985) for the El Nino winter of 1982-1983. This winter was unusual in that the heating region normally confined to Indonesia and the western Pacific had a much larger longitudinal extent, both east and west. The observed vorticity balances show a number of features which are in qualitative agreement with the theoretical model. For example the pushing apart of vorticity contours at upper level and the bunching together at lower level, as well as the sign of the meridional velocity in the heating region are as predicted by the theory.

However, a striking feature of the observations is the difference between the 150 mb balances and the 850 mb balance, due to the winds being much stronger at upper level than at lower level. One effect which can produce such an asymmetry is the compressibility of air. As a result of the weaker winds the relative vorticity at lower level is much smaller than the planetary vorticity. The observations are therefore well described by a <u>linear</u>

Sverdrup balance between the stretching and horizontal advection of planetary vorticity. At upper levels, on the other hand, the relative vorticity is of comparable magnitude to the planetary vorticity. To describe the upper level observations one needs a non-linear balance between the stretching and horizontal advection of total vorticity. The model used in this paper does not have the possibility of describing such a difference between the upper and lower levels.

Generally, the conclusions form the observational study support those deduced from theory. In particular, observations show that the vertical advection and twisting terms are small as the model finds, and the non-linear balances are better than the linear ones, also as the model finds. Another point of agreement is that outside the heating region, both sides of (9.2) are small i.e. there is little divergence and the flow is nearly parallel to the contours of total vorticity. This can be seen if figure 6(b) is superimposed on figure 4(b) and 7(b) is superimposed on figure 4(a) or 4(d).

To summarise, the conclusion is that non-linear effects are important, but the differences from linear theory are more in the way of a model distortion of the flow field rather than any qualitative change in behaviour. The weakly non-linear theory shows the nature of these distortions very well, the principle ones being at the western end of the heating region. These conclusions are supported by the numerical modelling work of Nobre (1983) and the observational study of Sardeshmukh and Hoskins (1985).

REFERENCES

Abramowitz, M. and Stegun, I.A. 1965 Handbook of Mathematical Functions, Dover, 1046 pp.

Gill, A.E. 1980 Some simple solutions for heat-induced tropical circulation, Quart. J.R. Met. Soc. 106, 447-462.

Gill, A.E. and Clarke, A.J. 1974 Wind-induced upwelling, coastal currents and sea-level changes, Deep-Sea Res. 21, 325-345.

Gill, A.E. and Rasmusson, E.M. 1983 The 1982-83 climate anomaly in the equatorial Pacific, Nature 306, 229-234.

Lau, K.M. and Lim, H. 1982 Thermally induced motion in an equatorial β-plane: Hadley and Walker circulation in the winter monsoon. Mon.Weath Rev. 110, 336-353.

Matsuno, T. 1966 Quasi-geostrophic motions in the equatorial area, J. Met. Soc. Japan, 44, 25-43.

Moura, A. and Shukla, J. 1981 On the dynamics of droughts in northeast Brazil. Observations, theory and numerical experiments with a general circulation model. J. Atmos. Sci. 38, 2653-2675.

Nobre, C.A. 1983 Tropical heat sources and their associated large-scale atmospheric circulation. PhD Thesis, Dept. of Meteorol and Phys. Oceanogr., M.I.T.

Sardeshmukh, P.D. and Hoskins B.J. 1985 Vorticity balances in the tropics during the 1982-1983 El Nino-Southern Oscillation event (to be published).

Silva Dias, P.L., Schubert, W.H. and DeMaria, M. 1983 Large-scale response of the tropical atmosphere to transient convection. J. Atmos. Sci. 40, 2689-2707.

Webster, P.J. 1972 Response of the tropical atmosphere to local steady forcing. Mon. Weath. Rev., 100, 518-541.

Figure captions

Figure 1. Schematic representation of the three flow regions in the limit of small damping. The heating is confined to the inner region $0<x<l$ The meridional scale a is the Rossby radius, and a/l is small but finite. The outer regions have a scale c/ν (where c is the wave speed and ν the function decay time) whose ratio with l tends to infinity.

Figure 2. The flow and pressure at the surface in the heating region in the linear inviscid limit. Values of y are given in units of Rossby radius. The solid lines are pressure contours, at intervals of $1/4\pi$. The arrows represent the winds, which are geostrophic (along pressure contours) and divergent. An arrow of unit velocity is drawn above the figure.

Figure 3. The flow and pressure at the surface in the outer regions in the linear limit. The solid lines are pressure contours, and the arrows represent the winds. In this outer region solution the heating region is seen as a discontinuity at x=o. The meridional scale is the Rossby radius, but the zonal scale is larger by a factor of $1/\epsilon$. (Contour interval of 0.15, arrow of unit length in the bottom right hand corner).

Figure 4. Contours of total vorticity, to $O(\zeta)$. The heating is concentrated in the region $0<x<\pi$ For an amplitude $\zeta = 0.45$ the vorticity is shown at $z = o$, the surface, in (a), and at $z = \pi$, the tropopause, in (b). For a vanishingly

Cont/d

small amplitude, δ =o, the contours reduce to straight lines, (c). Solid lines are used for positive values, dotted lines for the zero contour, and broken lines for negative values. x and y scaling in Rossby radii. (Contour interval = 0.3).

Figure 5. The non-linear corrections. Pressure contours and wind arrows for the barotropic correction (a), and the second baroclinic mode (b) at the surface z = o. Contouring conventions as in figure 4, with a contour interval of 0.15 and an arrow of unit length in the bottom right hand corner.

Figure 6. The flow at the surface z = o. In (a) the linear solution for infinitesimal heating, δ = o, and in (b) the non-linear solution for a finite amplitude, δ = 0.45. Contour intervals and arrows as in figure 5.

Figure 7. The flow at the tropopause, $z = \pi$. In (a) the linear solution, δ = o, and in (b) the non-linear solution, δ = 0.45. Contour maps of zonal velocity u as shown for (c) the linear case, δ = 0.45. Pressure contours and arrows as in figure 5, zonal velocity contours at intervals of 0.2.

Figure 8. The vertical velocity $w(z)$ in the middle of the heating region (x = 0.5, y = 0). The non-linear solution (solid line, δ = 0.45) is shifted upward relative to the heating and the linear solution (broken line, δ = 0).

Figure 9. Contours of the vortex stretching terms $(\frac{1}{2} y + \delta S)$ with the flow superimposed ($z = \pi$). In (a)

the linear solution, $\delta = 0$, and in (b) the non-linear solution, $\delta = 0.45$. (Contour interval of 0.1; arrow of unit length in the bottom right hand corner).

Figure 10. Sections along the equator, showing pressure (a), zonal velocity (b), and total head (c) at the surface. Solid lines are for the non-linear solution ($\delta = 0.45$), and broken lines for the linear solution ($\delta = 0$).

Figure 11. Sections along the western (solid lines) and eastern (broken lines) borders of the heating region. Pressure is shown on the left (i) and zonal velocity on the right (ii) for (a) the linear solution at the tropopause ($\delta = 0$, $z = \pi$), (b) the non-linear solution at the tropopause ($\delta = 0.45$, $z = \pi$), and (c) the non-linear solution at the surface ($\delta = 0.45$, $z = 0$).

Figure 12. The flow and pressure fields as simulated for a periodic domain by the method described in the text.

(a) $\delta = 0$, $z = 0$,
(b) $\delta = 0.45$, $z = 0$,
(c) $\delta = 0$, $z = \pi$,
(d) $\delta = 0.45$, $z = \pi$.

Contour intervals and arrows as in figure 5.

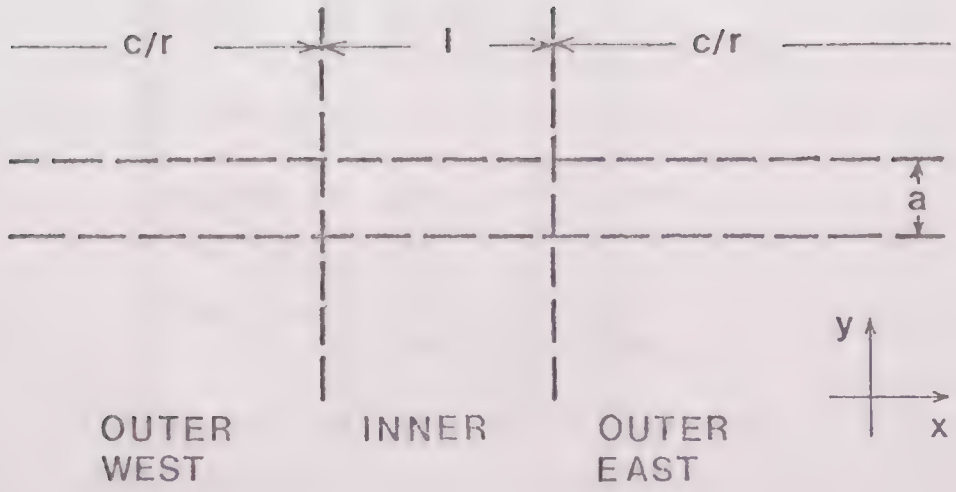

Fig 1

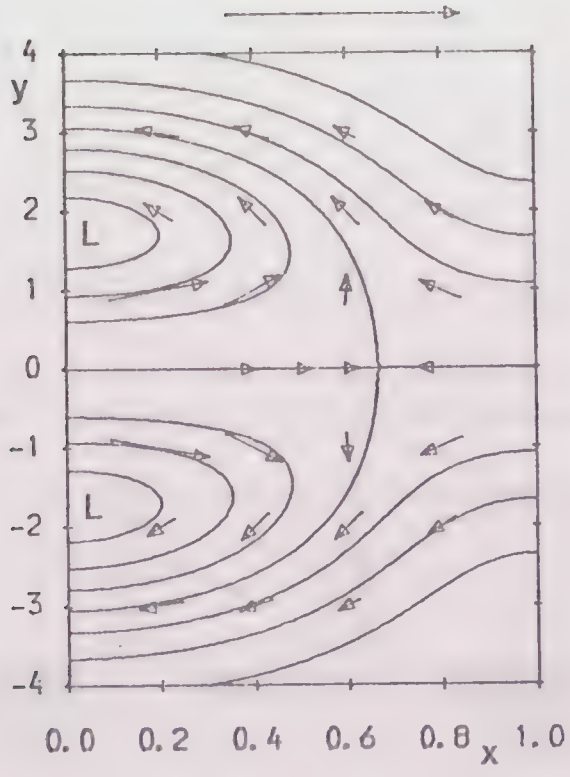

Fig 2

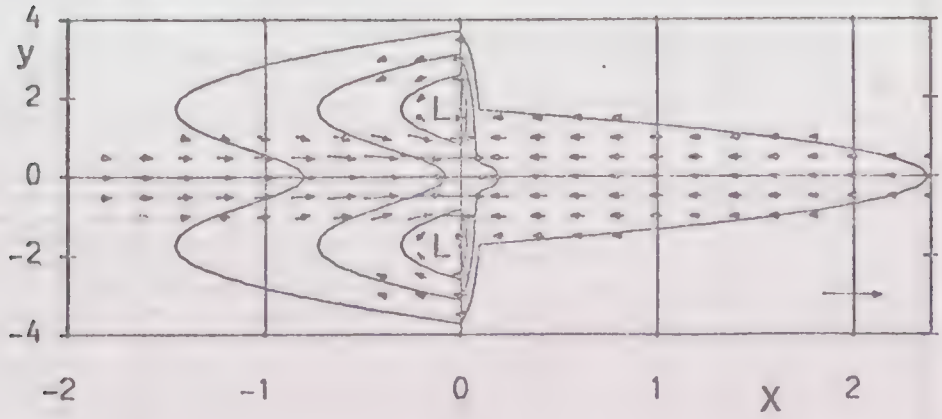

Fig 3

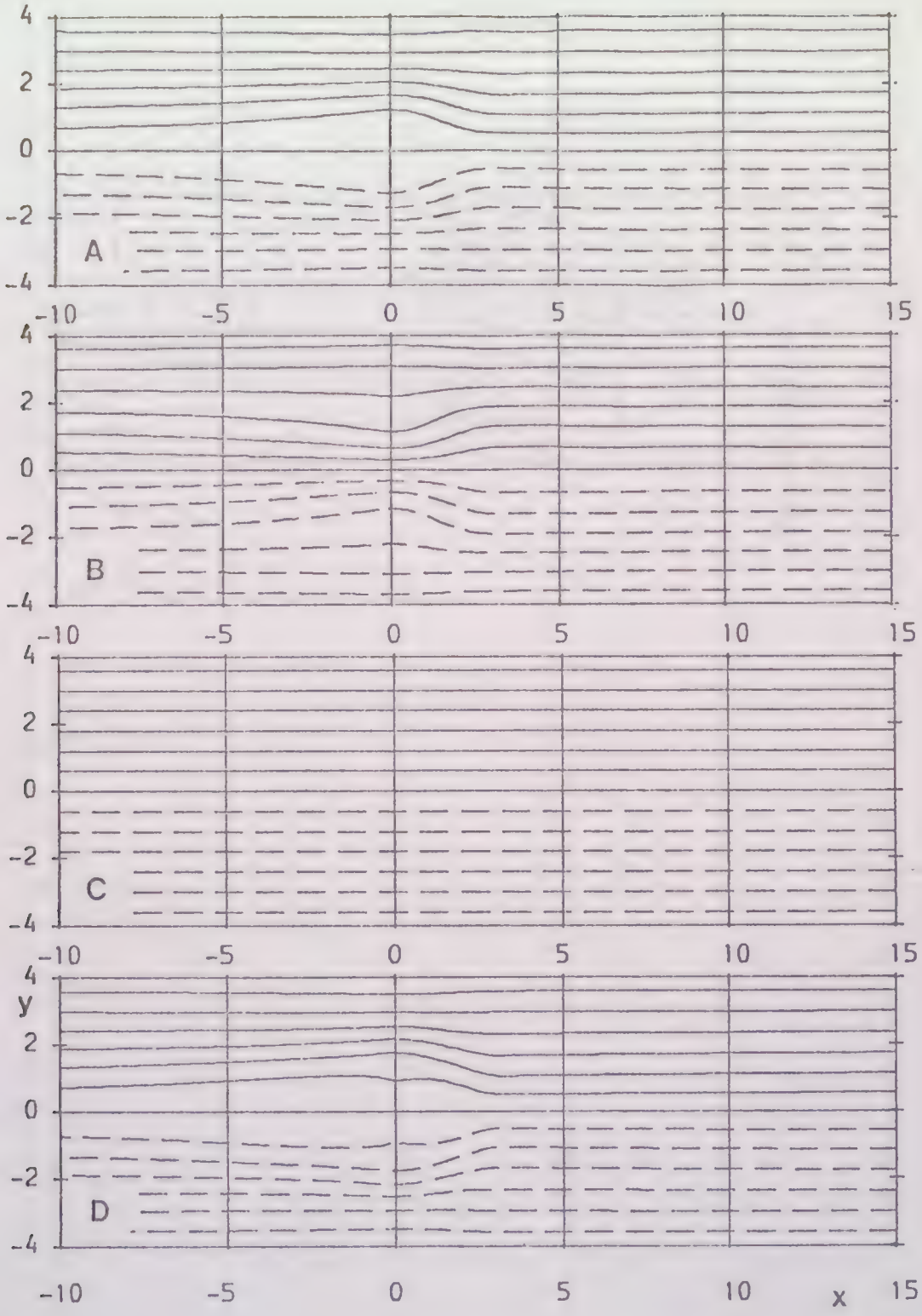

Fig 4

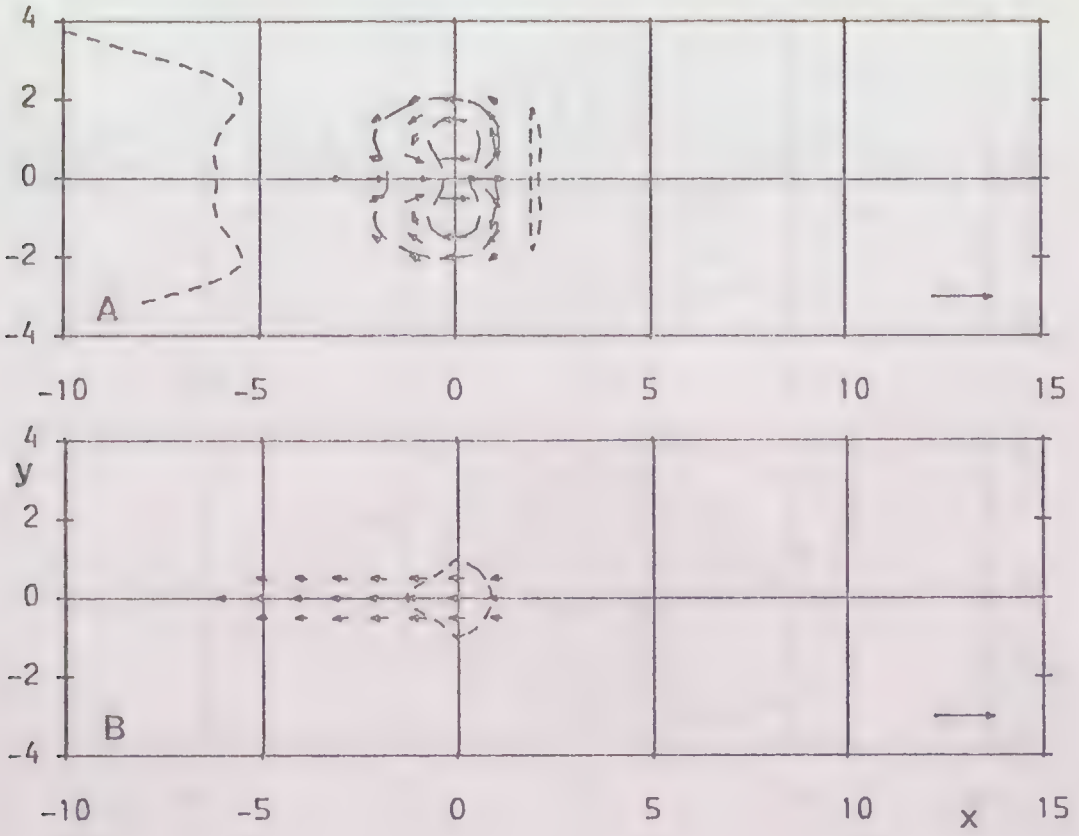

Fig 5

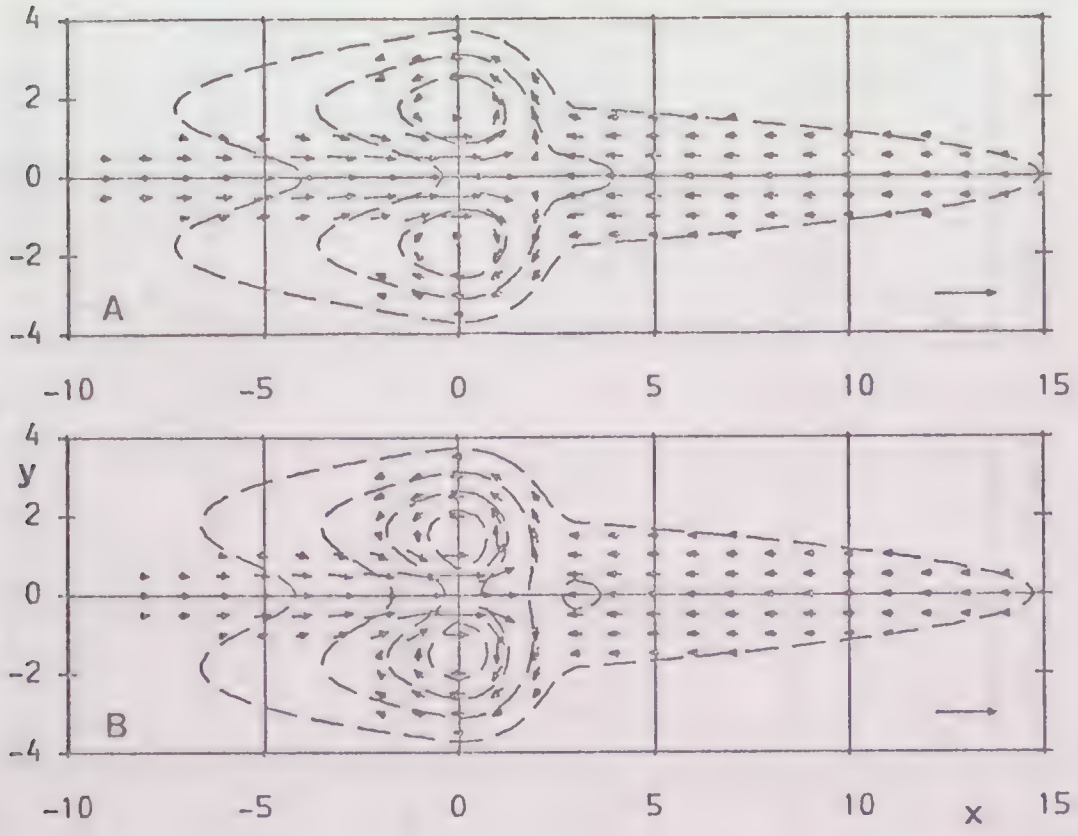

Fig 6

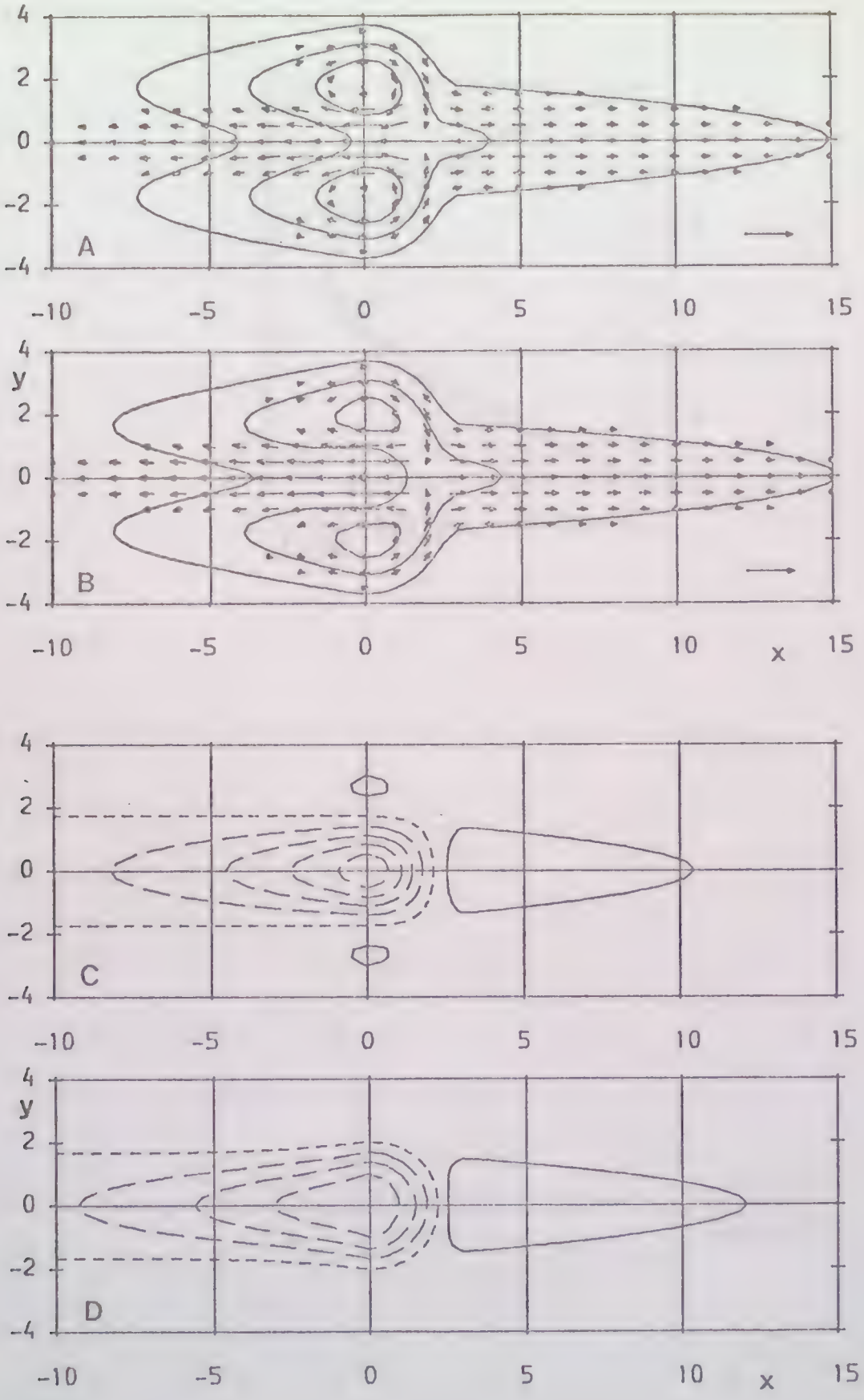

Fig 7

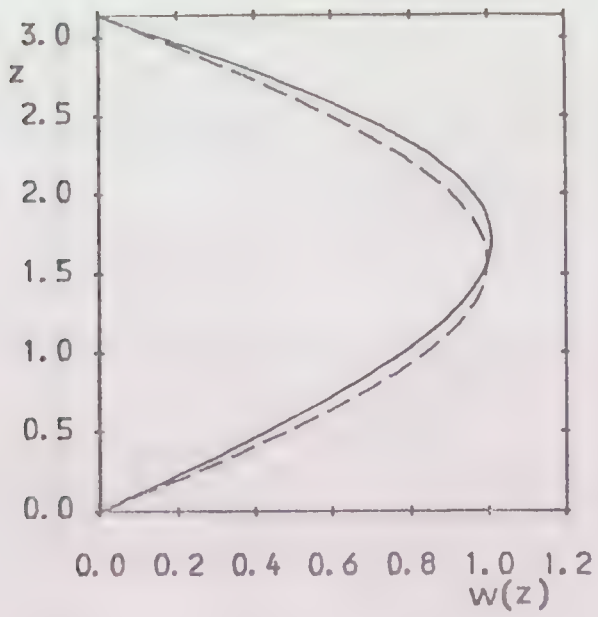

Fig 8

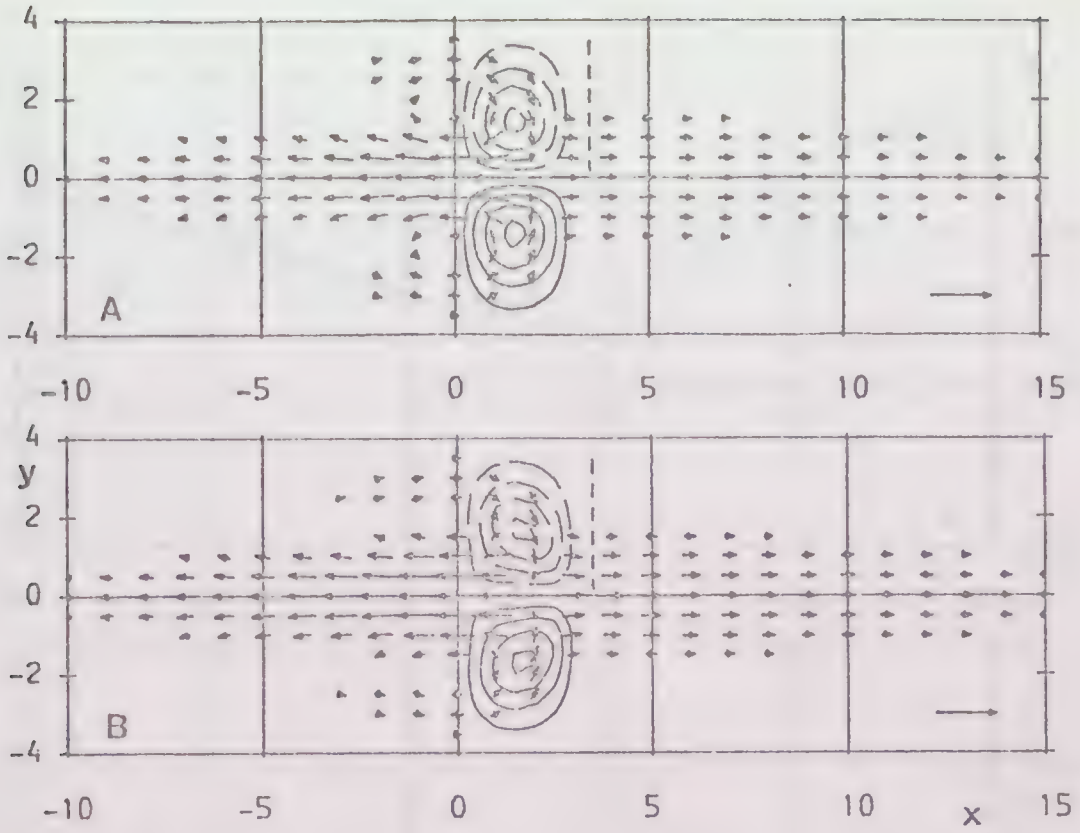

Fig 9

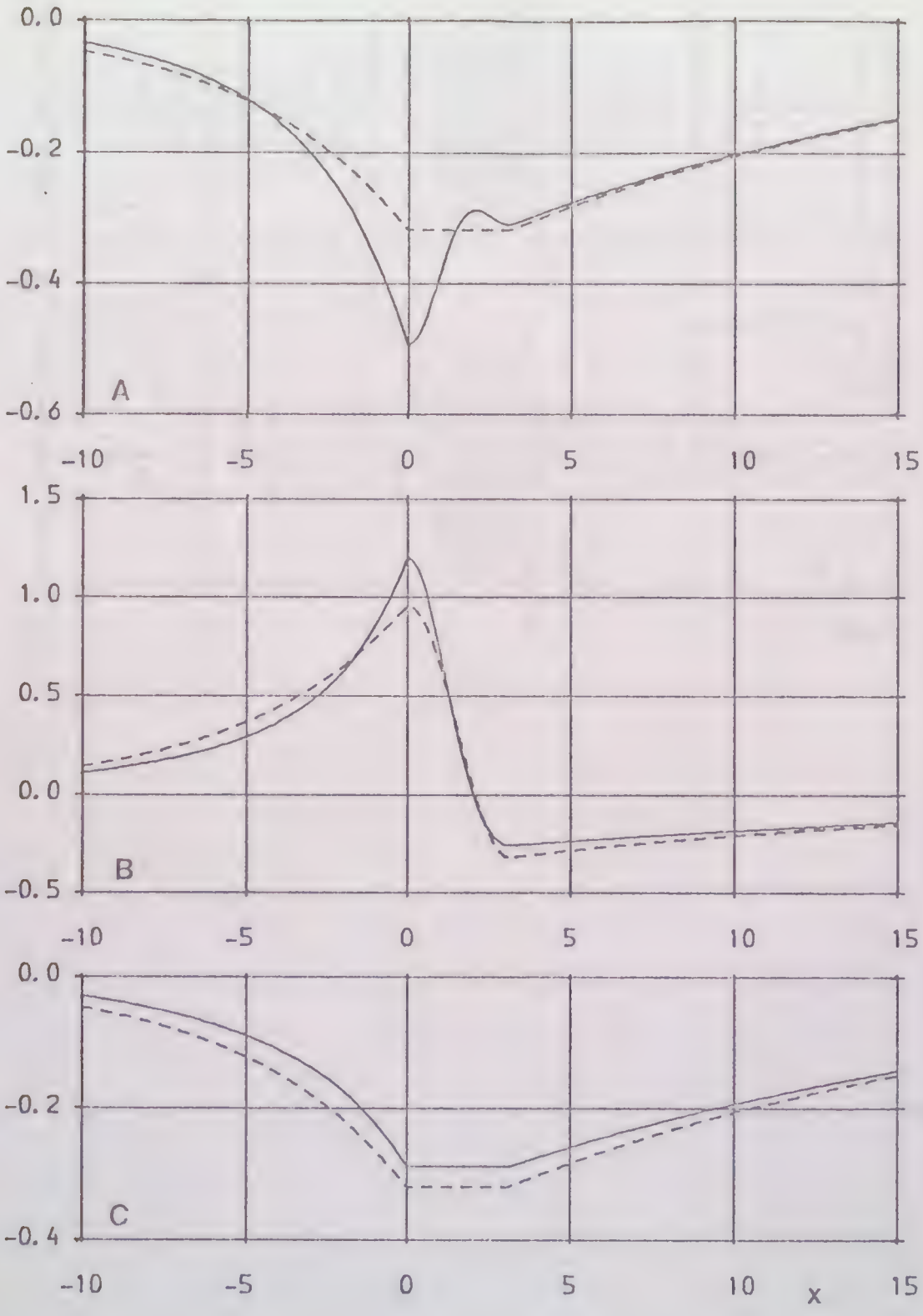
0.0
-0.2
-0.4
-0.6
A
-10
-5
0
5
10
15
1.5
1.0
0.5
0.0
-0.5
B
-10
-5
0
5
10
15
0.0
-0.2
-0.4
C
-10
-5
0
5
10
x
15

Fig 10

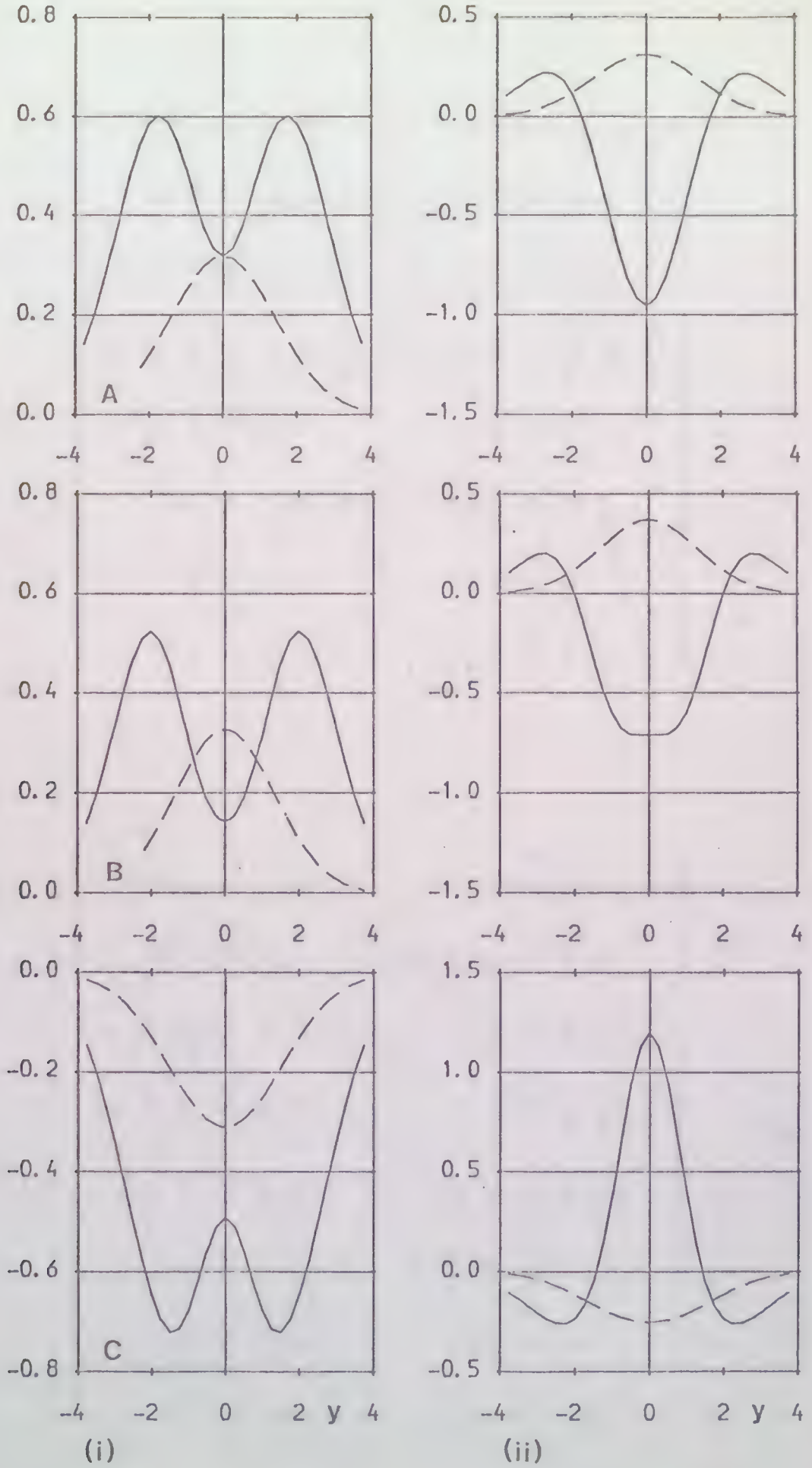

Fig 11

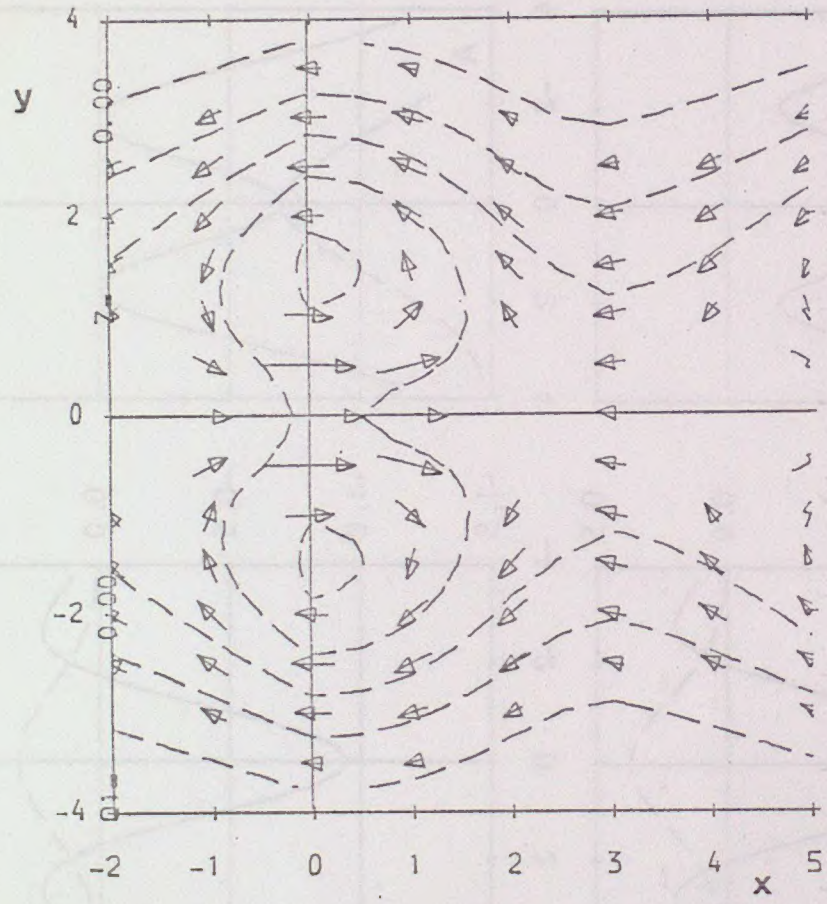

A

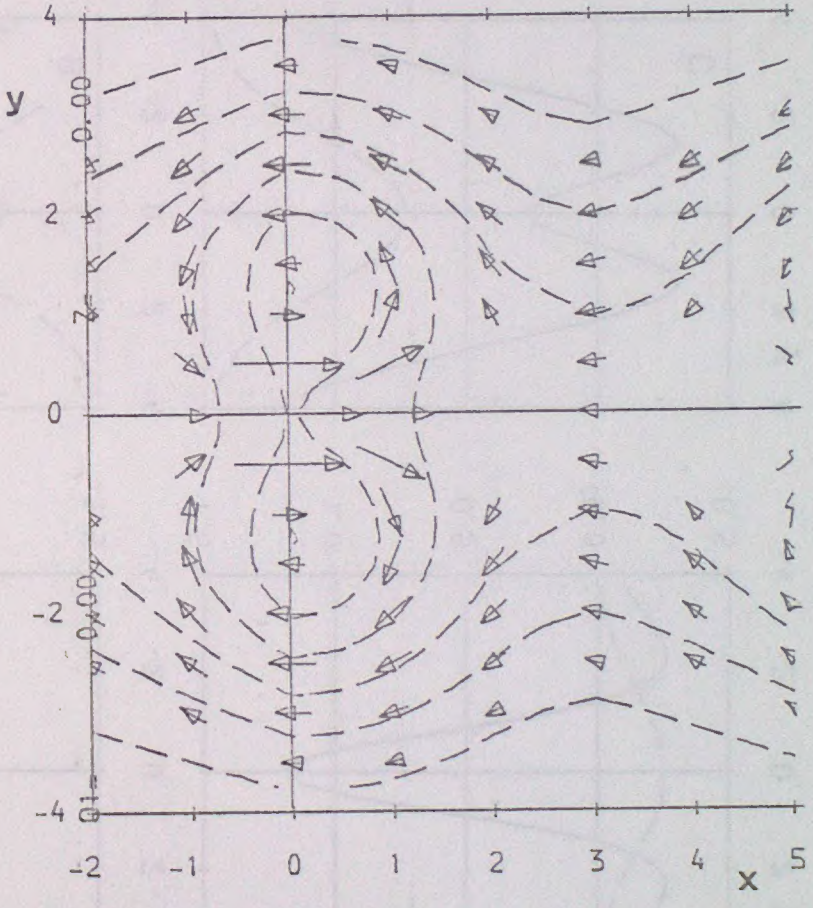

B

Fig 12

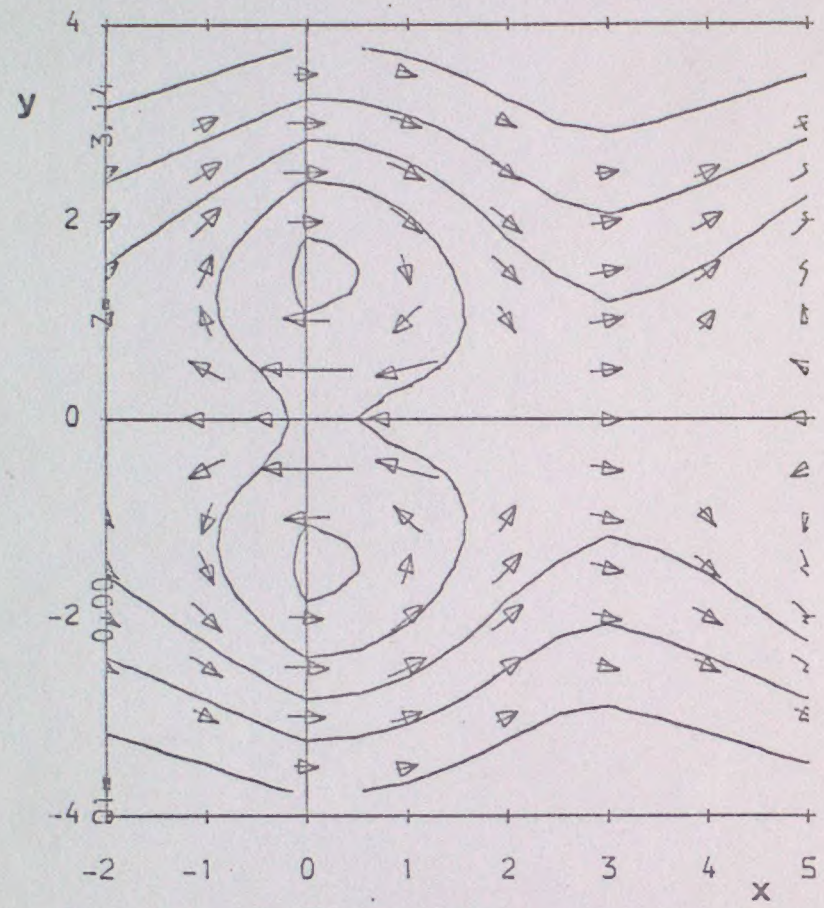

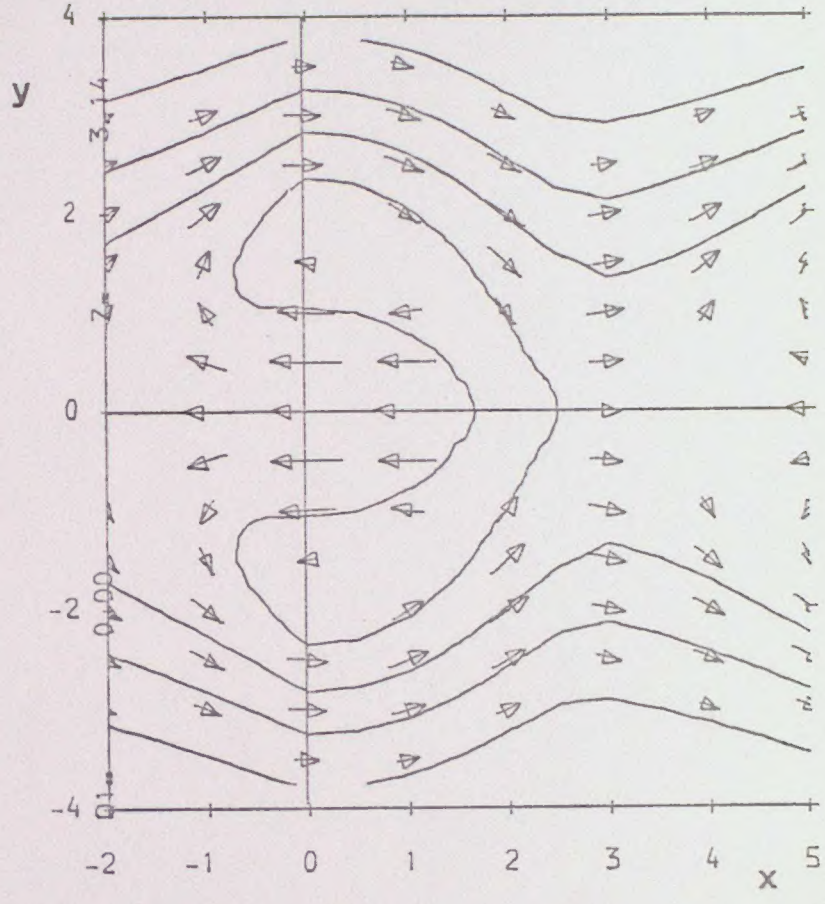

Fig 12

DYNAMICAL CLIMATOLOGY TECHNICAL NOTES

DCTN 1	June 1984	A scheme for incorporating the thermodynamic sea-ice model into a coupled ocean-atmosphere model. C Gordon and M Bottomley
DCTN 2	Sept 1984	The parametrization of the upper ocean mixed layer in coupled ocean/atmosphere models. C Gordon and M Bottomley
DCTN 3	Sept 1984	The response of a simple thermodynamic sea-ice model to GCM forcing appropriate for perennial sea-ice. M Bottomley
DCTN 4	Sept 1984	Potential vorticity in the stratosphere derived using data from satellites. S A Clough, N S Grahame and A O'Neill
DCTN 5	Sept 1984	Simulation of the seasonal cycle of SST using globally specified climatological data to force simple ocean models. N S Grahame
DCTN 6	Sept 1984	Development of an improved GCM radiation scheme. A Slingo and R C Wilderspin
DCTN 7	Sept 1984	On the specification of surface fluxes in coupled atmosphere/ocean general circulation models. J F B Mitchell, C A Wilson and C M Price
DCTN 8	Sept 1984	A survey of possible repercussions of the Soviet river reversal programme on Arctic sea-ice. H Cattle
DCTN 9	Oct 1984	A study of a strong stratospheric warming during January 1982 T D A Fairlie
DCTN 10	Nov 1984	An intercomparison of the Met O 11 N45 model and the Met O 20 11-level model on the Cyber 205 J F Dyson
DCTN 11	Nov 1984	Simulation of observed time series of temperature and precipitation over eastern England. D N Reed
DCTN 12	Nov 1984	Forecasts and analyses of the onset of the Southwest monsoon. R Kershaw
DCTN 13	Nov 1984	On modelling the effects of CO_2 on climate. J F B Mitchell
DCTN 14	Dec 1984	Development of a revised longwave radiation scheme for an atmospheric general circulation model. A Slingo and R C Wilderspin
DCTN 15	Jan 1985	Rossby wavetrains in the stratosphere forced by localised disturbances in the troposphere. C J Marks (Oxford), A O'Neill and V D Pope

DYNAMICAL CLIMATOLOGY TECHNICAL NOTES

DCTN 16	Jan 1985	Observing system experiments using the Meteorological Office's 15-level model. R A Bromley
DCTN 17	Feb 1985	Atmospheric general circulation simulation of the climate of the Mediterranean region. H Cattle
DCTN 18	Feb 1985	Diurnal variation and cloud in a general circulation model. C A Wilson and J F B Mitchell
DCTN 19	Feb 1985	The sensitivity of the Saharan region in a general circulation model. W M Cunnington and P R Rowntree
DCTN 20	Mar 1985	The impact of aircraft observations on analyses and forecasts from the operational 15-level model. B R Barwell